frontiers | Frontiers in Earth Science

TYPE Original Research
PUBLISHED 20 December 2024
DOI 10.3389/feart.2024.1520502

OPEN ACCESS

EDITED BY
Hu Li,
Sichuan University of Science and Engineering, China

REVIEWED BY
Caifang Wu,
China University of Mining and Technology, China
Yumeng Wang,
Helmholtz Association of German Research Centres (HZ), Germany

*CORRESPONDENCE
Baoqing Li,
19951233305@163.com

RECEIVED 31 October 2024
ACCEPTED 03 December 2024
PUBLISHED 20 December 2024

CITATION
Ye Z, Li B and Cao J (2024) Enrichment characteristics and genesis mechanism of critical elements (Nb-Ta-Zr-Hf-REE-Y) in coals: a case study of Late Permian coalfield in Northeastern Guizhou, China.
Front. Earth Sci. 12:1520502.
doi: 10.3389/feart.2024.1520502

Enrichment characteristics and genesis mechanism of critical elements (Nb-Ta-Zr-Hf-REE-Y) in coals: a case study of Late Permian coalfield in Northeastern Guizhou, China

Ziyi Ye, Baoqing Li* and Jialiang Cao

Key Laboratory of Tectonics and Petroleum Resources, China University of Geosciences, Ministry of Education, Wuhan, China

The discovery of coal-type beneficial metal deposits and corresponding genesis mechanisms are cutting-edge issues in current sedimentary environment research. Based on industrial analysis, mineralogy, and geochemical measurement of seven typical mines in the Late Permian coalfield of northeastern Guizhou, the enrichment characteristics and mineralization mechanisms of critical metal elements in coal rocks have been revealed in this study. The chemical composition of coal from the Late Permian Wujiaping Formation in northeastern Guizhou is mainly characterized by ultra-low moisture content, medium ash and medium volatile matter yield, and medium high sulfur content. The content of coal-hosted critical metal elements is very high. There are significant differences in elemental composition of coalbeds from different mines, and they are mostly enriched vertically in the coal between and near tonsteins. For example, the K1 coalbed of XX Mine is characterized by Se-Nb-Ta-Zr-Hf enrichment, while the K3 coalbed only has Se enrichment characteristics. TDY Mine has the characteristics of Zr-Nb-Be-Se-Hf-Ta and rare earth element (REE) -Y enrichment. The differences in assemblage type and abundance of critical metal elements in coal rock are mainly controlled by the input of terrestrial detrital materials, environmental conditions, seawater, and hydrothermal fluids. The weathering products of acidic volcanic ash, basalt, and intermediate acidic rocks in the Kangdian Upland provide material sources for the enrichment of critical metal elements. Specifically, the input of intermediate acidic volcanic ash is the main factor for the enrichment of Nb-Ta-Zr-Hf-REY (REE plus Y) in most coal mines. The coastal swamp environment in marine-continental transitional zone, periodic seawater transgression, and hydrothermal fluids control the alteration, transformation, and formation of detrital minerals, affecting the activation and migration of some critical metal elements.

KEYWORDS

late permian, critical elements, coal, terrigenous materials, volcanic ash, genesis mechanism

1 Introduction

Critical metal elements (including REY, Nb, Ta, Zr, Hf, Ga, Li, etc.) are valuable strategic resources that play important roles in industries such as new materials, energy, information technology, aerospace, and military industry (Zhai et al., 2019; Dai et al., 2022). Due to the growing demand and rising economic significance of these critical elements (Martin et al., 2017; Per and Erika, 2018), the demand for critical metals is increasing in recent years. In above context, the study of sedimentary deposits abundant with critical elements has received great attention from academic community of environmental science. As a sedimentary organic-rich rock with reduction and adsorption barrier properties, coal can serve as a carrier for the enrichment of various metal elements under special geological and geochemical conditions (Dai et al., 2012; Zhang et al., 2023). In terms of abundance, critical metal enrichment using coal as a carrier can even exceed that of traditional metal deposits (Zhao et al., 2019; Yang et al., 2017; Hower et al., 2019; Dai et al., 2020). Previous studies suggest that coalbeds, tonstein, roof, as well as other types of sedimentary rocks, volcanic ash altered clay rocks, and tuffs, can all enrich various strategic metals, forming a scale for industrial exploitation (Zhou et al., 2023; Dai et al., 2022; Dai et al., 2024; Jin et al., 2024).

The enrichment of trace elements in coal can be summarized into following models: terrestrial detrital enrichment model, tuff enrichment model, infiltration or atmospheric groundwater driven model, and exudation enrichment model related to fluid rise of various origins (Seredin and Finkelman, 2008). The genesis types of strategic metallic minerals in coalfields are complex. As of now, various genesis types including volcanic ash type, volcanic ash-hydrothermal alteration composite type, syngenetic or epigenetic hydrothermal leaching type, submarine exhalation type, hydrothermal-sedimentary environment composite type, etc., Have been reported successively (Crowley et al., 1993; Dai et al., 2005; Dai et al., 2012; Dai et al., 2022; Liu et al., 2019). The total coal resources in the northeast Guizhou coalfield are not abundant compared with those in the northern, western and southwestern parts of Guizhou (Zhang et al., 2023), but several mining areas in coals are highly enriched in critical elements, with higher average than those of Chinese coal (Dai et al., 2012), such as REY (573 μg/g)-Nb (90 μg/g)-Ta (9 μg/g)-Zr (869 μg/g)-Hf (18 μg/g)-Ga (48 μg/g)-Li (110 μg/g). In addition, the abundance of critical metal elements in the coal of Northeast Guizhou has obvious spatiotemporal heterogeneity, which is manifested in the fact that the abundance of elements in different coal seams in the same coal seam and in different mining areas is very different, which has become a key factor restricting the research for rich ore horizons. As for the causes of the enrichment of critical elements in coals in the late Permian of Guizhou, many scholars have put forward their own opinions. Ren (2006) and Dai et al. (2012) suggested that terrestrial detrital materials are one of the main controlling factors for mineral and trace element anomalies in coal in southwestern China, and the terrestrial input of Emeishan basalt from the Kangdian Upland has a significant impact on the enrichment of critical elements in the late Permian coals from western Guizhou (Wang et al., 2012; Shen et al., 2023). The volcanic ash input, hydrothermal activity after deposition, and alteration of acidic fluids have been proposed to control the enrichment of critical metals in coal in north and northwest Guizhou (Li et al., 2020; 2022; Jin et al., 2024). Zhang et al. (2023) summarized the research results of coal geochemistry in Guizhou in the past 20 years and concluded that the enrichment of Nb, Ta, Zr, Hf and REY in Late Permian coal is mainly affected by the supply of weathering products from Emeishan basalt, the mixing of syn-diagenetic volcanic ash and low-temperature hydrothermal activity after coal deposition.

The coal-bearing strata of the Late Permian coalfield in northeastern Guizhou were not affected by volcanic activity during depositional process, and the coupling enrichment of REE-Nb-Ta-Zr-Hf-Ga cannot be attributed to conventional tuff type enrichment mechanism (Dai et al., 2024). The spatiotemporal heterogeneity of critical metal element abundance has not been thoroughly studied. Controlling factors for the spatiotemporal heterogeneity, and the coupling relationship between geological controlling factors and the critical metal element enrichment remain unknown. Based on mineralogy, and geochemical measurement of seven different mines in the Late Permian coalfield of northeastern Guizhou, the objectives of this study are to reveal the coupling relationship between geological factors and critical element enrichment and to determine mechanism of element enrichment and mineralization.

2 Geological setting

The Late Permian coalfield in northeastern Guizhou Province is located in the Central Yangzi Plate (Figure 1A). During the Middle Permian, under extensive transgression, thick shallow marine carbonate formations (Maokou Formation and Qixia Formation) were deposited in southwest China. To the beginning of Late Permian, influenced by the Dongwu Movement, seawater retreated to deep water basins in southern Guizhou, and most of the northeastern part of Guizhou rose to land and altered by weathering. Meanwhile, a large-scale basaltic magma eruption occurred in the northwest of Guizhou Province, and formed Emeishan Large Igneous Province (ELIP). The ELIP can be divided into three zones: inner zone, middle zone and outer zone. The inner zone is the central position of the mantle plume of Emeishan, and the huge thick Emei basalt is deposited in the inner zone, forming a topographic plateau, namely, the Kangdian Upland (Figure 1B). After the large-scale Emei basalt eruption, influenced by basement subsidence and hot and humid climate, large-scale coal accumulation began in the southwest China of the early Late Permian (Li et al., 2022).

The ELIP had a significant controlling effect on the Late Permian coal-hosted rare metal deposits in southwestern China (Figure 1B). These controlling effects are manifested in the following four aspects: 1) The topography formed by ELIP (high in the west and low in the east) provides favorable conditions for peat accumulation, leading to the distribution of most coal-bearing strata in the middle and outer zones of ELIP; 2) The Kangdian Upland is a positive tectonic unit located in the western part of Guizhou, extending in a north-south direction, and has become the main provenance area in Northeastern Guizhou. 3) The volcanic ash generated by the weakening of mantle plume activity can serve as a basis for peat accumulation (forming the bottom of coal seams) or terminate peat accumulation (forming the

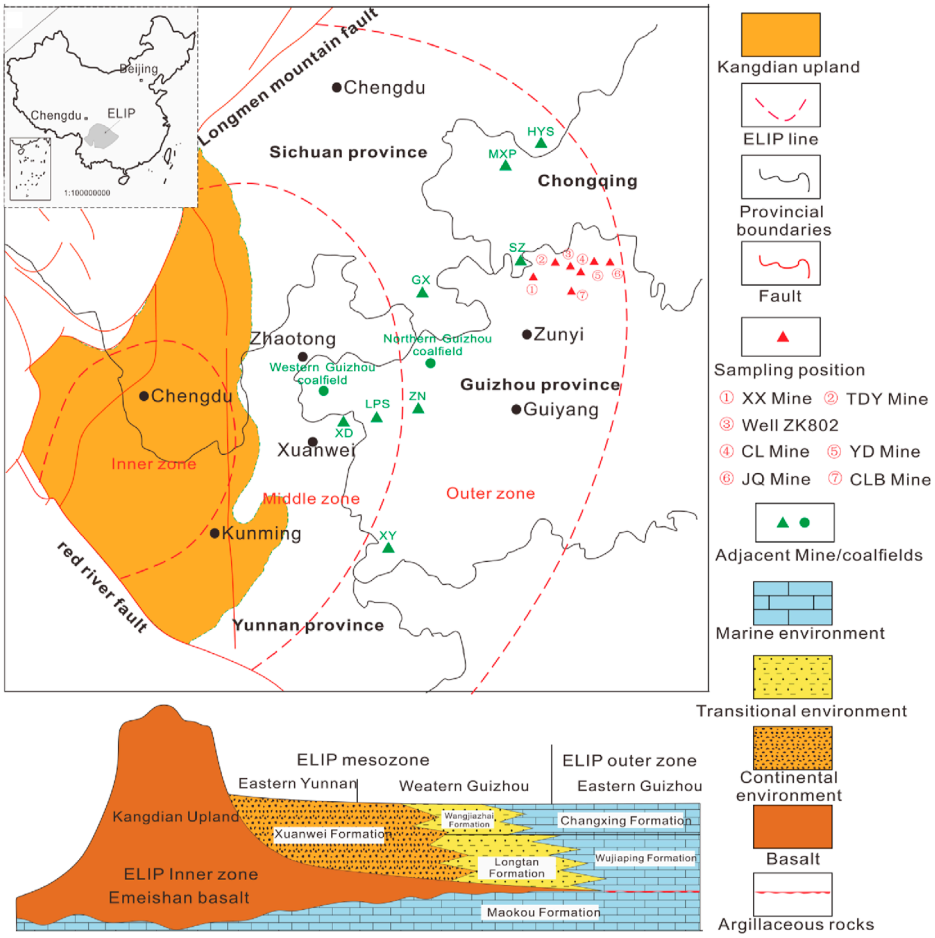

FIGURE 1
Distribution of inner, intermediate, and outer zones of the Emeishan Large Igneous Province (ELIP) and location of the study area [modified after He et al. (2003); Shen et al. (2021)].

roof of coal seams); 4) Frequent volcanic activity and related hydrothermal activity are conducive to the accumulation of organic matter in the Late Permian coal-bearing strata in South China (China Coal Geology Bureau, 1996; Li et al., 2020).

In the middle zone of ELIP, the Maokou Formation limestone, Emeishan basalt and coal bearing rock series (Xuanwei Formation or Longtan Formation) formed an accumulation sequence from bottom to up. In the outer zone, the Maokou Formation limestone, argillaceous rock and coal bearing rock series (Wujiaping Formation) constitute a stacking sequence (Figure 1B). The coal-bearing strata studied belong to the Upper Permian Wujiaping Formation, which is a set of shallow marine sediments. The lithology of Wujiaping Formation includes carbonate rocks interbedded with siliceous rocks and clastic rocks (Figure 2A). Two coalbeds are identified, one of which has commercial value for mining. In the early Late Permian, Wujiaping belonged to the transgression period, with the direction of transgression from southeast to northwest. The seawater moved back and forth frequently, forming a lithofacies paleogeographic feature consisting of continental facies-transitional facies-marine facies from northwest to southeast (China Coal Geology Bureau, 1996).

3 Methodology

3.1 Samples

The coal and non coal samples collected in this study were from K1 and K3 Coalbed of XX Mine in the Late Permian coalfield of northeastern Guizhou, as well as the 4th Coalbed of CL Mine, TDY Mine, JQ Mine, YD Mine, CLB Mine, and the drilling core of Well ZK802. The location of sampling points is shown in Figure 1A. A total of 77 samples were collected, including 62 coal samples, 6 tonstein samples, and 9 roof (or floor) samples (Figure 2B).

3.2 Analytical techniques

Firstly, the collected samples are crushed step by step. Then conduct industrial analysis, total sulfur analysis, mineralogical and geochemical analysis on the processed samples. According to ASTM Standard D3173/D3173M-17a (2017), ASTM Standard D3174-12 (2018), and ASTM Standard D3175-17

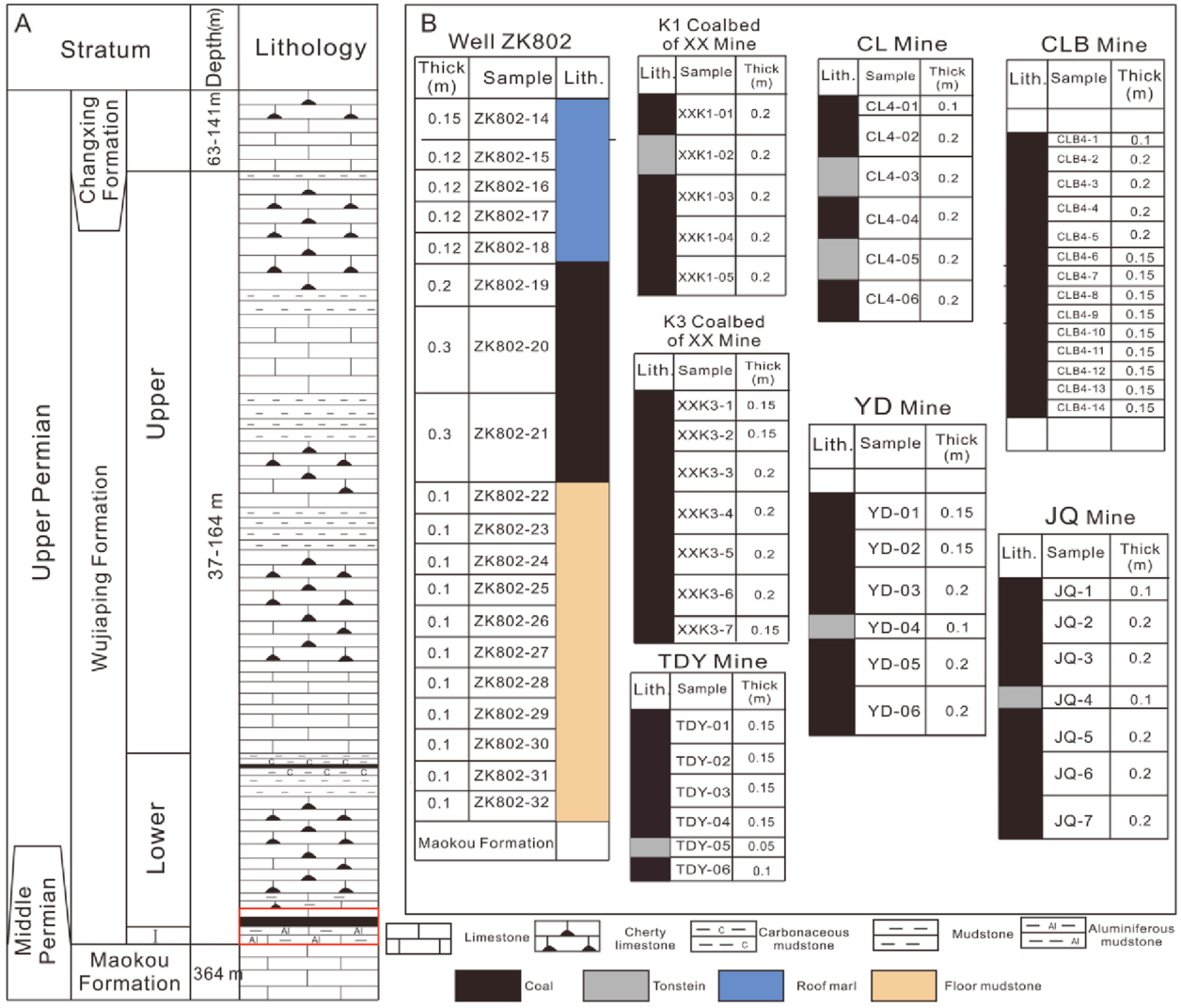

FIGURE 2
(A) Stratigraphic column of the Late Permian in northeast Guizhou, the red box indicates the layer of sampling location. **(B)** The quantity and distribution of collected samples in different mining areas of the Late Permian coalfield in northeast Guizhou.

(2011), the moisture content, ash yield, and volatile matter yield of coal and tonstein were measured. Use Bruker D8 A25 Advance powder diffractometer to scan the X-ray spectrum of samples. Qualitative identification of mineral phases was carried out using PDF-2 and EVA software (Bruker), and semi-quantitative analysis of mineral content was performed using normalized reference intensity ratio (Chung, 1974). Utilizing a field emission scanning electron microscope (FE-SEM, FEI Quanta) equipped with energy dispersive X-ray spectroscopy (EDS; Genesis Apex 4) ™ 450 FEG), to determine the morphological characteristics of minerals and the distribution of elements in minerals. Use Thermo's ARL ADVENT'XP+X-ray fluorescence spectroscopy (XRF) to determine the content of major elements. According to the two-step digestion method proposed by Querol et al. (1997), the sample was digested and the content of trace elements and rare earth elements was determined using inductively coupled plasma-mass spectrometry (ICP-MS, X-Series II Thermo). The experimental steps are as follows:

Step 1: Weigh 0.1 g of the sample and place it in a polytetrafluoroethylene (PFTE) tank. Add 2.5 mL of HNO_3 to the sample, cover it with a lid, and place it in a constant temperature incubator at 90°C for at least 4 h. Transfer the obtained solution to a 100 mL centrifuge tube and clean the dissolution tank with deionized water to recover the samples. Ensure that all samples enter the centrifuge tube and centrifuge at 3,000 rpm for 20–25 min;

Step 2: Remove the upper clear liquid and place it in a conical flask. The solid residue was recovered using 2.5 mL of HNO_3, poured into the previous PFTE tank, and 7.5 mL of HF (2.5 mL, 2.5 mL, 2.5 mL) was added again. All solid samples were recovered into the PFTE dissolution tank. Place the dissolution tank in a constant temperature chamber at 90°C and maintain it for 24 h. Place the dissolution tank on a heating plate (230°C) for acid quenching operation, and add 2.5 mL of $HClO_4$ during this process. After the liquid has

evaporated, add 1 mL of HNO_3 and evaporate again. After evaporation, 1 mL of HNO_3 was added for sample recovery, and the dissolution tank was cleaned with deionized water. All the liquid was poured into the previous conical flask, and then diluted to 100 mL with deionized water to obtain a 2.5% HNO_3 solution for ICP-MS analysis.

3.3 Principal component analysis (PCA) method

PCA is a multivariate data analysis technique that can be used to capture much of the information in a large multi-dimension data matrix in fewer dimensions (Meglen, 1992; Iwamori et al., 2017). One of its main applications is to reveal relationships among variables (Yamashita and Tanoue, 2003; Boehme et al., 2004), since it chooses the new axes to lie along directions of highest correlation (Gotelli and Ellison, 2004). The projection of each variable on the new axis is called its loading, which indicates the relative importance of each variable on that axis; the projection of each sample in the new axis is called its score (Meglen, 1992). PC is a linear combination of variables, with the first sample of all samples being scored on the first axis, the second sample being scored on the second axis, and so on. PCs are orthogonal to each other (right angles: "orthogonal" is a dimensional analogy of "vertical") and are therefore not correlated. In this article, we use an Origin 2022 program to build PCAs. The detailed introduction and use method can be referred to Xue et al. (2011).

4 Results

4.1 Coal quality characteristics

The measurement results of moisture content, ash content, volatile matter yield, and sulfur content of coal samples from different mines are shown in Table 1. The moisture content ranges from 0.7% to 4.1%, with most results distributed between 1.0% and 1.5% and an average of 1.5%, indicating that the coal sample belongs to ultra-low moisture coal (MT/T 850-2000, 2000). The ash content ranges from 7.4% to 69.9%, concentrated between 15% and 30%, with an average of 22.14%. According to GB/T 15224.1–2018, it belongs to low ash to medium ash yield coal. The yield of volatile matter is mostly distributed in a range of 15%–29%, with an average of 21.9%, belonging to low volatile to medium volatile bituminous coal (MT/T849-2000, 2000). The ash yield of coal samples shows a good positive correlation with the yield of volatile matter (R^2 = 0.65), indicating that the yield of volatile matter is influenced by inorganic components. The total sulfur content ranges from 1.1% to 24%, with an average of 4.4%. According to the classification criteria for sulfur content in coal by Chou. (2012), coal samples in this study are mainly composed of medium and high sulfur coal (>3%). There is a good positive correlation between sulfur content and ash yield (R^2 = 0.48–0.97), especially in high sulfur samples (R^2 of 0.85, 0.96, 0.96 for CLB, XX, and CL coal mines, respectively). It is suggested that sulfur in coal mainly exists in inorganic components, such as sulfide minerals (pyrite), sulfate minerals, etc. (Finkelman, et al., 2018; Finkelman, et al., 2019).

4.2 Mineral characteristics

4.2.1 Mineral compositions and contents

The coal samples in this study are composed of clay minerals (including kaolinite, illite, ammonium illite, and zeolite), oxide minerals (quartz and rutile), sulfide minerals (pyrite and sphalerite), carbonate minerals (calcite, dolomite, and siderite), and sulfate minerals (gypsum, pyrite) (Figure 3). Taking the coal sample from the CLB Mine as an example, pyrite (2.4%–38%) is the main mineral component, followed by ammonium illite (0%–5.8%) and a small amount of kaolinite (0%–4.4%) (Table 2).

The mineral content of the tonstein sample differs from that of the coal sample. In the TDY Mine, the main mineral type of tonstein is kaolinite (60%), followed by pyrite (1.2%). Kaolinite is the main mineral (51%) in the YD Mine, and contains trace amounts of pyrite (0.88%). In the CL mine, the main mineral of tonstein is kaolinite (with an average value of 51%), followed by pyrite (with an average value of 2.6%) and a small amount of calcite (with an average value of 1.2%). Tonstein in the JQ Mine is mainly composed of kaolinite (65%), followed by illite (4.4%). Only kaolinite (75%) and a small amount of rutile (4.8%) were detected in tonstein samples from the K1 coalbed of XX Mine.

4.2.2 Mineral distribution and occurrence characteristics

Kaolinite is the main clay mineral in coal samples, occurring in strip or lens-shaped (Figures 4A, B). Kaolinite can also serve as a matrix for pyrite, rutile, and quartz particles (Figures 4C, D). A small amount of kaolinite is a fracture-filling cement (Figure 4A), formed by precipitation of aluminum and silicon-containing solutions. A small amount of kaolinite appears in the organic matter cell lumens (Figure 4C), indicating syndiagenetic-early diagenetic origin. Worm-like kaolinite may be of volcanic ash origin (Figure 4E). Illite has a low content and is often present as a cell-filling cement for microscopic components (Figures 4F, I), or dispersed in granular form in organic matter (Figure 4G).

In some samples, quartz and illite are co-filled in the cell lumens and micro-fractures of organic matter (Figure 4F), indicating a authigenic origin. In other samples, quartz occurs in granular form in organic matter matrix or kaolinite matrix (Figure 4G). The long axis of this type of quartz is parallel to the bedding plane and has a certain degree of roundness, belonging to terrigenous detrital origin. Calcite occurs in fractures or vein forms in organic matter (Figure 4H). It is suggested that calcite precipitates directly from Ca-rich hydrothermal fluids. In floor samples, calcite occurs in granular form in the kaolinite matrix (Figure 4M). Siderite is only observed in coal samples from the YD Mine and JQ Mine, filling the organic pores in an irregular shape (Figure 4J), suggesting a hydrothermal precipitation origin.

The occurrence forms of pyrite include 1) subeuhedral to euhedral crystal aggregates (Figures 4D, E); 2) Cell lumen-filling cement (Figure 4K); 3) Spherical polycrystalline framboidal (Figure 4I); 4) Other granular forms in organic matter matrix or kaolinite matrix (Figure 4P); 5) The fracture-filling cement (Figure 4L) is of hydrothermal origin.

The forms of gypsum occurrence include euhedral crystals (Figure 4N) and fracture-filling cements (Figure 4K). Gypsum clusters are concentrated near pyrite or iron sulfate, indicating that they are

TABLE 1 Industrial analysis and total sulfur analysis results of coal samples from 7 mines of the Late Permian coalfield in northeast Guizhou. (Mad, moisture; Ad, ash yield; V_{daf}, volatile matter; S, total sulfur; ad, air-dried basis; d, dry basis; daf, dry and ash-free basis).

Mine/Well	Coalbed	Sampling quantity			Industrial analysis results			S (%)
		Coal	Tonstein	Roof (or floor)	M_{ad} (%)	A_d (%)	V_{daf} (%)	
CLB	4th	14			0.7–1.8 (1.33)	7.4–40.6 (15.7)	12.8–26.37 (15.35)	2.3–24.1 (7.0)
TDY	4th	5	1		1–1.7 (1.33)	11.5–62.1 (26.48)	17–35.4 (22.58)	1.3–2.7 (1.88)
YD	4th	5	1		0.9–4.1 (1.76)	16.7–27 (21.38)	19.3–26.9 (22.34)	1.1–7.5 (2.5)
CL	4th	4	2		1–1.9 (1.3)	17.5–30.4 (21.23)	18.9–20.2 (22.75)	1.8–5.2 (3.08)
JQ	4th	6	1		0.9–2.4 (1.67)	7.7–69.9 (30.96)	16.7–33.6 (24.57)	1.5–11 (3.33)
XX	K1	3	1		1.3–2.4 (1.65)	19.1–40.2 (30.35)	13.8–18.9 (16.6)	3.2–6.3 (5)
XX	K3	7			0.9–2.0 (1.74)	13.2–34.9 (18.13)	12.6–21.1 (15.21)	1–16 (5.07)
ZK802	4th	3	11	5	1.2–1.4 (1.33)	22.8–23.9 (23.33)	19.8–29 (23.57)	1.9–2.9 (2.33)

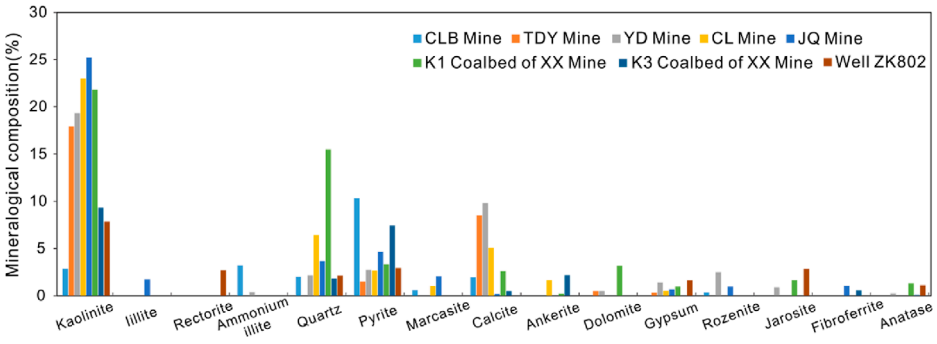

FIGURE 3
Mineral compositions of coal samples from the Late Permian coalfield in northeast Guizhou.

TABLE 2 Mineral compositions of coal samples from the Late Permian coalfield in northeast Guizhou. (Kln, Kaolinite; Qz, Quartz; Py, Pyrite; Cal, Calcite; Ank, Ankerite; Dol, Dolomite; Gyp, Gypsum; Roz, Rozenite; Jar, Jarosite; Fib, Fibroferrite; Mar, Marcasite; Ana, Anatase; Amm, Ammonium illite; Rec, Rectorite).

Mine/Well	Kln	Qz	Py	Cal	Ank	Dol	Gyp	Roz	Jar	Fib	Mar	Ana	Amm	Ilt	Rec
CLB	2.87	2.00	10.32	1.94				0.36			0.59		3.20		
TDY	17.93		1.49	8.48		0.50	0.31								
YD	19.35	2.15	2.74	9.80		0.51	1.39	2.47	0.88			0.25	0.38		
CL	23.00	6.42	2.65	5.06	1.64		0.52				1.00				
JQ	25.21	3.67	4.63	0.19			0.70	0.95		1.04	2.05			1.71	
XX (K1 Coalbed)	21.82	15.48	3.35	2.60	0.22	3.17	0.96		1.64			1.29			
XX (K3 Coalbed)	9.32	1.81	7.44	0.51	2.17					0.57		0.09			
ZK802	7.87	2.13	2.93				1.63		2.83			1.10			2.70

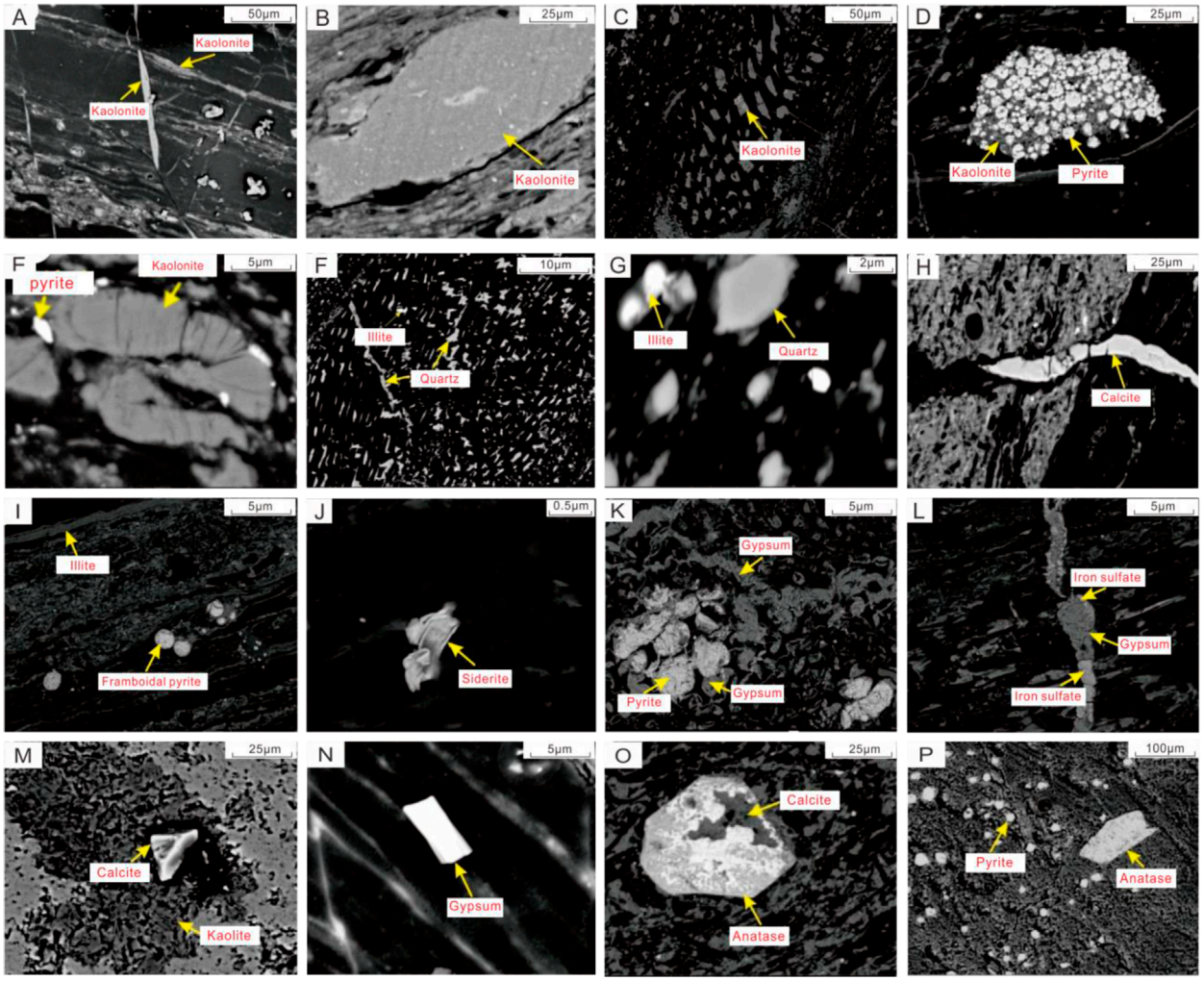

FIGURE 4
SEM back scattered images of different mineral phases from the Late Permian coalfield in northeast Guizhou. **(A)** Striped-shaped kaolinite filled fractures **(B)** Lens-shaped kaolinite; **(C)** Kaolinite cement in the cell lumen; **(D)** Pyrite in the kaolinite matrix; **(E)** Worm-like kaolinite and pyrite; **(F)** Illite and quartz filling the cell lumen, and quartz filling the organic fractures; **(G)** Granular illite and semi-rounded quartz; **(H)** Calcite filled in fractures; **(I)** Striped-shaped illite and strawberry-shaped pyrite; **(J)** Irregular-shaped siderite; **(K)** Pyrite filling the cell lumen and gypsum filling the fractures; **(L)** Gypsum and iron sulfate fill fractures; **(M)** Calcite in kaolinite matrix; **(N)** Euhedral gypsum crystals; **(O)** Euhedral rutile crystal; **(P)** Granular pyrite and rutile in organic matter.

likely formed by the interaction between sulfuric acid formed by the oxidation of pyrite and calcite (Figure 4L). A small amount of rutile is distributed in small dispersed particles in the organic matter matrix (Figure 4P), indicating that rutile originates from the reprecipitation of Ti-rich solution. Anatase occurs as cylindrical form in the kaolinite matrix. Low roundness of the anatase indicates its terrigenous detrital origin. There are dissolved spaces in the self-shaped crystal rutile, which are filled with kaolinite (Figure 4O), indicating the influence of hydrothermal solutions.

4.3 Geochemical characteristics

4.3.1 Major element oxides

The average content and proportion of major element oxides are shown in Table 3 and Figure 5A. The distribution of major elements in different coal mines exhibits strong heterogeneity. Taking CLB Mine as an example, its major elemental composition is Fe_2O_3 (7.05%), followed by SiO_2 (5.0%) and Al_2O_3 (2.96%). Compared with the average value of Chinese coal (Figure 5B), Si, Al, K, and Ti are more enriched in coal samples in this study, especially in the K1 Coalbed of XX Mine and the 4th Coalbed of Well ZK802. Fe, Na, and other minerals are relatively depleted, especially TY and YD Mines. Furthermore, Ca is depleted in the 4th coal seam of JQ Mine, K3 Coalbed of XX Mine, and the 4th Coalbed of ZK802 well, but is more enriched in TYD Mine and CL Mine. K is only depleted in the K3 Coalbed of XX Mine.

4.3.2 Trace elements enrichment

According to the enrichment coefficient proposed by Dai et al. (2012) (CC = element content/average trace element content in coal worldwide), the enrichment levels of critical metal elements are

TABLE 3 Average of major element oxides (%) from the Late Permian coalfield in northeast Guizhou (based on bulk samples). *, data of average values for Chinese coals (Dai et al., 2012).

Mine/Well	SiO_2	Al_2O_3	CaO	Fe_2O_3	K_2O	MgO	Na_2O	P_2O_5	TiO_2
CL	16.92	7.53	2.40	3.30	0.30	0.35	0.10	0.10	0.35
JQ	13.36	6.77	0.11	2.89	0.39	0.17	0.10	0.10	0.43
TYD	13.28	6.97	3.18	1.00	0.30	0.27	0.10		0.38
XXK1	22.54	7.68	0.90	5.36	0.35	0.42	0.28	0.10	1.16
YD	9.52	8.80	2.48	2.50	0.35	0.25	0.10		0.40
XX (K3 Coalbed)	7.94	3.61	0.39	5.83	0.10	0.10	0.10		0.31
ZK802	33.22	26.50	0.38	5.05	0.71	0.41	0.10	0.10	2.97
Chinese coals*	8.47	5.98	1.23	4.85	0.19	0.22	0.16	0.09	0.33

TABLE 4 Average of trace element (μg/g) in northeast Guizhou and adjacent coalfields/coal mines in the Late Permian (on whole coal or rock basis). 1, data of average values for Chinese coals (Dai et al., 2012); 2, data of average values for world hard coals (Ketris and Yudovich, 2009).

Mine/Well/coalfield	Se	Zr	Nb	Mo	Hf	Ta	Th	U	REY
XX (K1 Coalbed)	7.5	290	42	3.6	6.6	2.0	9.6	4.2	303
XX (K3 Coalbed)	11	104	17	2.1	2.8	1.3	6.5	1.9	96
CLB	9.9	67	10	16	1.6	0.06	2.5	4.5	105
TDY	7.4	468	49	6.9	9.7	1.8	9.1	6.0	347
CL	14	987	77	7.5	17	0.68	8.4	6.5	534
YD	14	820	81	4.5	18	5.7	19	6.5	621
JQ	16	886	62	23	16	2.7	12	15	660
ZK802	8.4	384	61	9.5	9.5	2.7	13	6.6	374
North Guizhou coalfield	1.0	162	26	2.0	2.4	0.90	6.0	2.5	111
ZN	3.2	173	22	7.2	2.6	3.2	5.4	9.3	136
LPS	3.6	141	15	4.8	2.2	2.3	4.6	5.2	89
XY	1.8	162	19	39	2.5	0.80	4.5	17	109
West Guizhou coalfield	2.8	157	19	12	2.4	2.3	4.9	7.5	98
MXP	66	411	43	6.5	11	2.9	12	376	423
GX	4.9	410	38	2.5	7.4	1.5	6.8	15	276
XD	6.6	112	11	1.8	3.0	0.92	7.1	2.1	465
SZ	13	444	24	3.7	9.9	1.8	9.4	18	460
HYS	7.0	695	76	4.1	10	0.68	8.5	4.1	1,423
Chinese coals[1]	2.47	89.5	9.44	3.08	3.71	0.62	5.84	2.43	117.69
World hard coals[2]	1.3	36.00	3.70	2.2	1.2	0.28	3.3	2.40	60.07

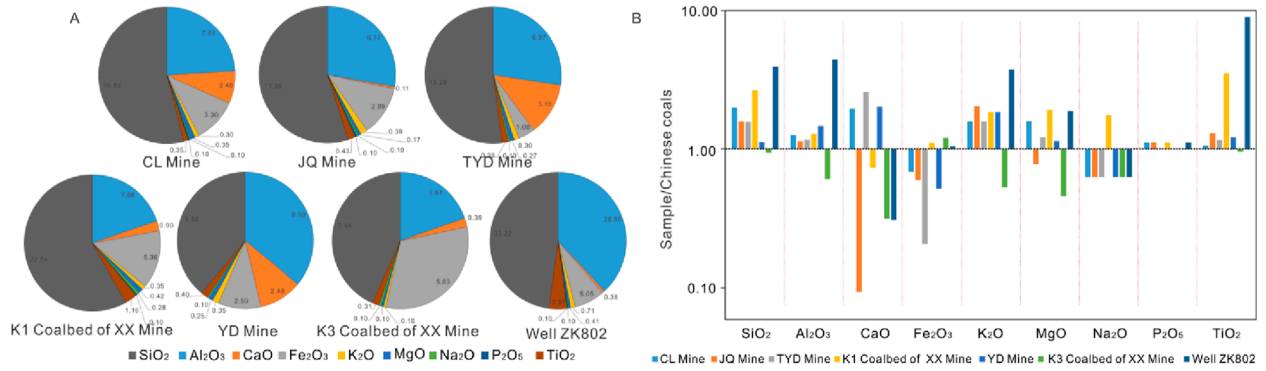

FIGURE 5
(A) Mineral compositions of the Late Permian coalfield in northeast Guizhou. **(B)** Concentration coefficient of major element oxides for coal samples from the Late Permian coalfield in northeast Guizhou.

divided into six categories: CC<0.5 (depleted), 0.5<CC<2 (normal), 2<CC<5 (slightly enriched), 5<CC<10 (enriched), and 10<CC<100 (highly enriched) (Figure 6). The K1 Coalbed of XX Mine is mainly enriched in Se-Nb-Ta-Zr-Hf, while the K3 Coalbed of XX Mine shows Se enrichment. TDY Mine is enriched in both Zr-Nb-Be-Se-Hf-Ta and REY. CL Mine exhibits enrichment characteristics of Zr-Nb-Be-Se-REY-Hf-Ta. The YD Mine is characterized by enrichment of Se-Zr-Hf-Nb-Ta-REY-Be-Th, while the JQ Mine is characterized by enrichment of Se-Zr-Hf-Nb-Ta-REY-Mo-U. CLB Mine is characterized by Se-Mo-U enrichment. The coal samples from Well ZK802 have Se-Nb-Ta-Zr-Hf-REY-Mo-U-V enrichment, with a higher degree of enrichment of critical elements compared to samples from coal mines.

The Late Permian coalfields in northeastern Guizhou have enriched elements such as Nb, Ta, Zr, Hf, REY, Se, Th, and U to varying degrees, these enrichment element combinations were also found in adjacent coalfields/coal mines, such as MXP Mine, HYS Mine, SZ Mine, XD Mine, Northern Guizhou and Western Guizhou coalfields, etc. In addition, there were certain differences in the combination and content of enrichment elements among different mines in northeastern Guizhou coalfields (Table 4).

For example, the Zr content ranges from 8.9 to 3,083 μg/g, with an average value of 393 μg/g, far higher than the world hard coal (average value of 36 μg/g). It is also higher than the average value of Zr in XD, LPS, ZN, XY Mine and Northern Guizhou, Western Guizhou coalfields (<200 μg/g), slightly lower than the content of Zr in MXP, GX and SZ Mine (>400 μg/g), and lower than that in HYS Mine (695 μg/g). In the three coal mines of CL, YD, and JQ, the average value of Zr is relatively high, at 987 μg/g, 820 μg/g, and 886 μg/g, respectively. In the coal samples collected from the CLB Mine, the degree of Zr enrichment is the lowest (average value of 67 μg/g), but still higher than the Zr content in the world hard coal.

Figure 7 shows that critical metal elements such as Li, Nb, Ga, and REY are most enriched in or near tonstein, while their enrichment in roof (or floor) samples is relatively weak. The variation trends of Al2O3, ash content, kaolinite, and critical metal elements are basically consistent (Figure 7), indicating that detrital input is the main factor controlling the enrichment of trace elements.

4.3.3 Rare earth element and yttrium (REY) enrichment

The average REY content of coal samples from JQ and YD coal mines was the highest, at 660 μg/g and 621 μg/g, respectively (Table 5), followed by CL Mine. Compared with the other coalfields in Guizhou, the coal in the northeastern Guizhou coalfield is more enriched in REY. Compared with the coal samples from adjacent Mines, the content of REY is significantly lower in HYS, lower than that of MXP, SZ and XD (423 μg/g, 460 μg/g and 465 μg/g), and higher than the average content of REY in GX (276 μg/g). From the continental environment in the western study area to the marine environment in the east, there is a trend of increasing REY content in coal, which is related to the influence of terrestrial input on peat deposition (Zhuang et al., 2000). The classification and enrichment types of REY were based on the classification scheme proposed by Seredin and Dai (2012). Taking the K1 Coalbed of XX Mine as an example, LREY ranges from 157 to 328 μg/g (average 263 μg/g), and MREY ranges from 34 to 68 μg/g (average 52.0 μg/g). HREY ranges from 12 to 6.3 μg/g (average 9.4 μg/g), and LREY content is significantly higher than MREY and HREY. The δEu value ranges from 0.42 to 0.37, indicating a significant negative Eu anomaly. δCe ranges from 0.77 to 1.01, showing a weak negative Ce anomaly. Except for one sample characterized by weak negative La anomaly (<1), all other samples exhibit positive La anomalies (1.08–1.15). All samples showed varying degrees of positive anomalies in Gd (1.11–2.83).

As shown in the REY curves of K1 Coalbed in XX Mine (Figure 8A), the REY content of tonstein (Sample No. XXK1-2) is significantly higher than that of other samples. XXK1-2, XXK1-4, and XXK1-5 exhibit LREY enrichment with $La_N/Yb_N>1$. XXK1-1 and XXK1-3 exhibit MERY enrichment, with $La_N/Sm_N<1$ and $Gd_N/Yb_N>1$. Tonstein (Sample No. XXK1-2) showed significant negative Ce anomalies, while the rest samples had normal or weak negative Ce anomalies. All samples exhibit Eu negative anomaly. The REY characteristics of coal samples from other coal mines/drilling wells are shown in Figure 8. The coals of Well ZK802 occur weakly negative Eu anomalies only (Figure 8H), this may be explained by the influence of high-temperature hydrothermal solutions (Hower et al., 2015; Zhou et al., 2023).

FIGURE 6
Concentration coefficients (CC) of trace elements from the Late Permian coalfield in northeast Guizhou.

5 Enrichment mechanism of critical elements

5.1 Control of terrestrial input

5.1.1 Using PCA to determine the impact of terrigenous detrital inputs

Terrigenous detrital input has a significant controlling effect on the abnormal enrichment of minerals and trace elements in coal in southwest China (Ren, 2006; Dai et al., 2012; Shen et al., 2023). In order to determine whether terrigenous detrital input has an effect on the enrichment of key elements in coal in this area, principal component analysis (PCA) was used to explore the relationship between sulfur content, ash content, mineral composition and geochemical elements in coal (Figure 9). Based on the ordination diagram Figure 9A, we noted that the loadings angle of the variables in red dotted box such as Zr, Al_2O_3, REY, Ga, Hf, Ta, etc., is very small, and the projection value on the *X*-axis (PC1) is significantly larger and closer, while Mo, U, Fe_2O_3, Se has a larger projection value on the *Y*-axis (PC2). This indicates that the sources and genesis of Zr, Al_2O_3, REY, Ga, Hf, Ta, etc., Are similar, and they are obviously affected by terrestrial sources, but the enrichment of U, Mo, Se and Fe elements was of non-terrigenous origin. Similarly, we find that the kaolinite and ash content in Figure 9B are projected on PC1 with high values, which also proves that the enrichment of these elements in the red dotted box is obviously influenced by terrigenous detritus. In addition, we find that the loadings of sulfur content and pyrite content in Figure 9B are very close, and the projection value on PC2 is higher, which indicates that most of the sulfur in coal originates from pyrite, and also proves that the enrichment of U, Mo, Se is related to pyrite and sulfur.

5.1.2 Basalt debris input from Kangdian Upland

The weathering products of ELIP in Kangdian Upland provide the main provenance of terrestrial input for the Late Permian coalfields in Yunnan and Guizhou provinces in SW China, and are an important basis for the enrichment of REY and trace elements in coals (Yang et al., 2011; Shen et al., 2021). In this study, Al_2O_3-TiO_2, Zr/TiO_2-Nb/Y, and Zr-Ti cross-plots were applied to discuss the influence of basaltic provenance in the Kangdian Upland on the Late Permian coalfields (Figure 10). The Al_2O_3/TiO_2 ratio can be used to determine the magma source of altered volcanic ash in coal-bearing strata. Hayashi et al. (1997) proposed that Al_2O_3/TiO_2 ratios ranging from 3–8, 8–21, and 21–70 respectively indicate the presence of ferromagnesian, neutral rock, and felsic provenance. Winchester and Floyd (1977) found the abundance and distribution of selected minor, trace elements (Ti, Zr, Y, Nb, Ce, Ga and Sc) and their cross-plot may be used to distinguish common volcanic rock types. Although elements including Al, Ti, Nb, and Y, can be relatively mobile in a few specific supergene environments (Ward, 2016; Dai et al., 2015). The Al_2O_3/TiO_2-Nb/Y, Zr-Ti and Zr/TiO_2-Nb/Y

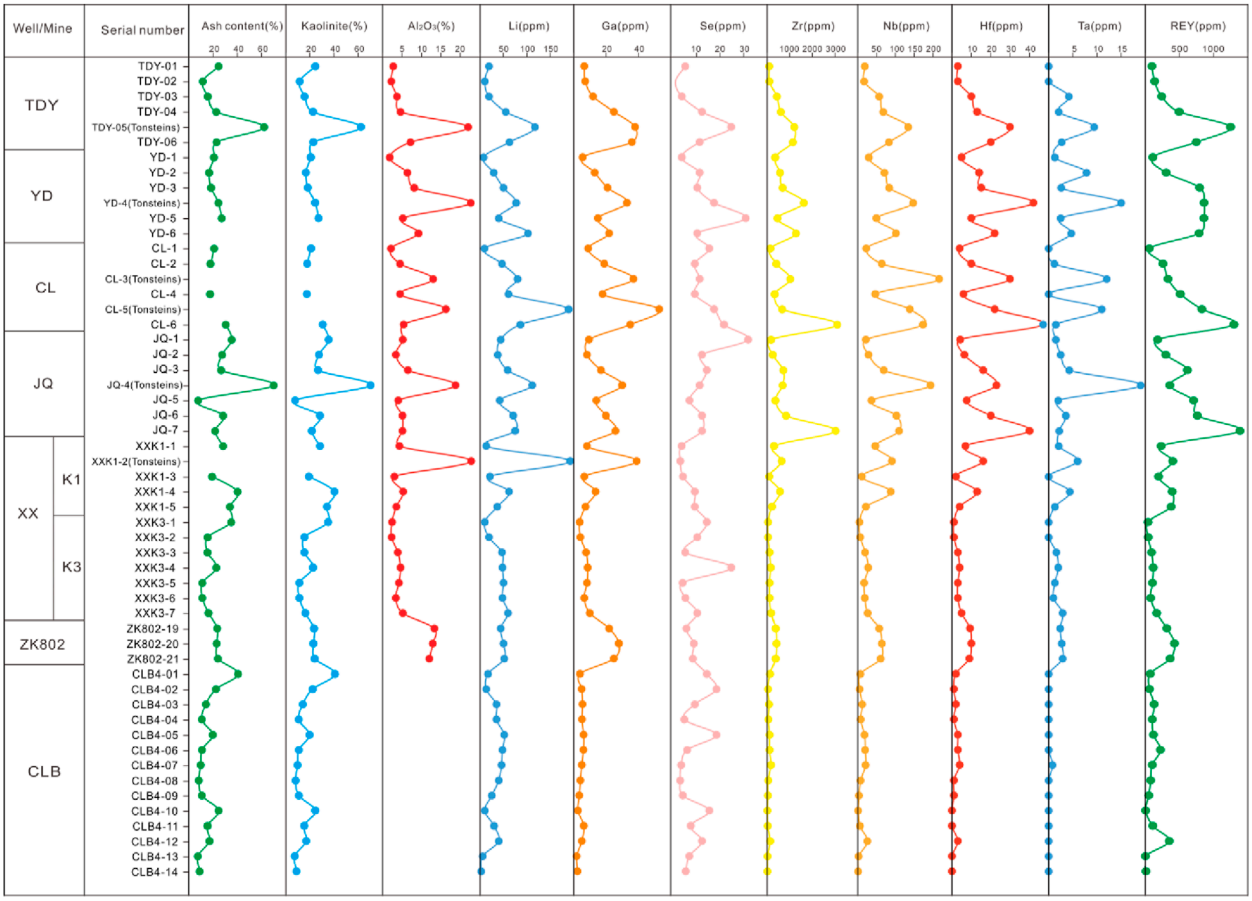

FIGURE 7
Variations of ash, kaolinite, Al_2O_3, REY, and critical trace element contents of the Late Permian coalfield in northeast Guizhou.

TABLE 5 REY geochemical parameters of coal and tonstein samples in the Late Permian coalfield in northeast Guizhou. L, M, and H are light, medium, and heavy REY; $(La/Yb)_N$, $(La/Sm)_N$, $(Gd/Yb)_N$ are the standardized ratios; N, Upper Continental Crust Normalized; $\delta Eu = Eu_N/(Sm_N + Gd_N)^{0.5}$; $\delta Ce = Ce_N/(La_N + 0.5Pr_N)^{0.5}$; $\delta La = La_N/(3Pr_N - 2Nd_N)^{0.5}$; $\delta Gd = Gd_N/(0.33Sm_N + 0.67Tb_N)^{0.5}$.

	REY (μg/g)	LREY (μg/g)	MREY (μg/g)	HREY (μg/g)	δCe	δEu	δLa	δGd	$(La/Yb)_N$	$(La/Sm)_N$	$(Gd/y)_N$
XX (K1 Coalned)	324.00	262.80	51.80	9.34	0.93	0.72	1.08	1.47	1.44	1.03	1.39
XX (K3 Coalbed)	95.57	75.43	17.71	2.34	0.96	0.75	1.17	3.12	1.10	0.96	1.15
CLB Mine	105.60	85.86	17.40	2.52	1.24	0.61	1.21	2.64	1.32	1.08	1.23
TDY Mine	497.17	378.00	99.17	20.18	1.10	0.38	1.05	1.82	0.86	0.75	1.21
CL Mine	550.17	423.33	104.83	22.10	1.05	0.31	1.04	1.46	0.95	0.84	1.08
YD Mine	621.00	469.67	125.67	25.98	1.04	0.38	1.13	1.10	0.84	0.86	1.02
JQ Mine	617.57	452.29	139.14	26.24	1.03	0.39	1.12	1.40	1.22	1.02	1.23
Well ZK802	373.33	308.33	54.00	11.33	0.90	0.89	1.10	0.98	1.30	0.98	1.13

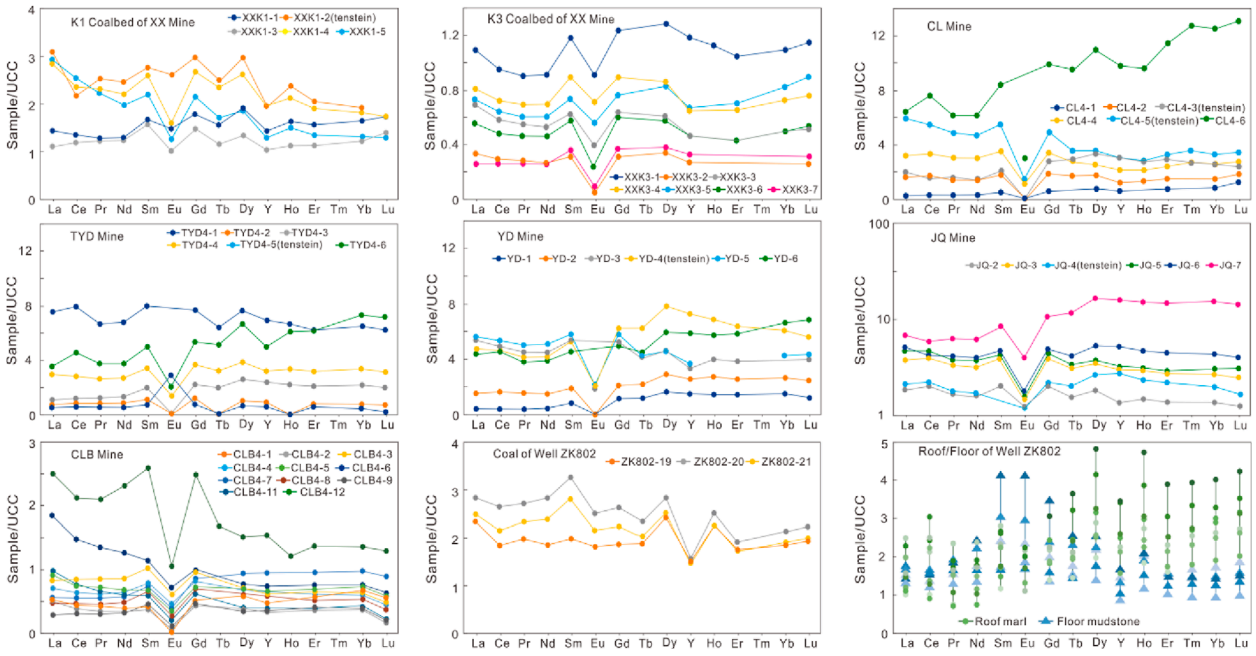

FIGURE 8
REY distribution patterns in the coal, roof, and floor samples from the Late Permian coalfield in northeast Guizhou. UCC are cited from Taylor and McLennan. (1985).

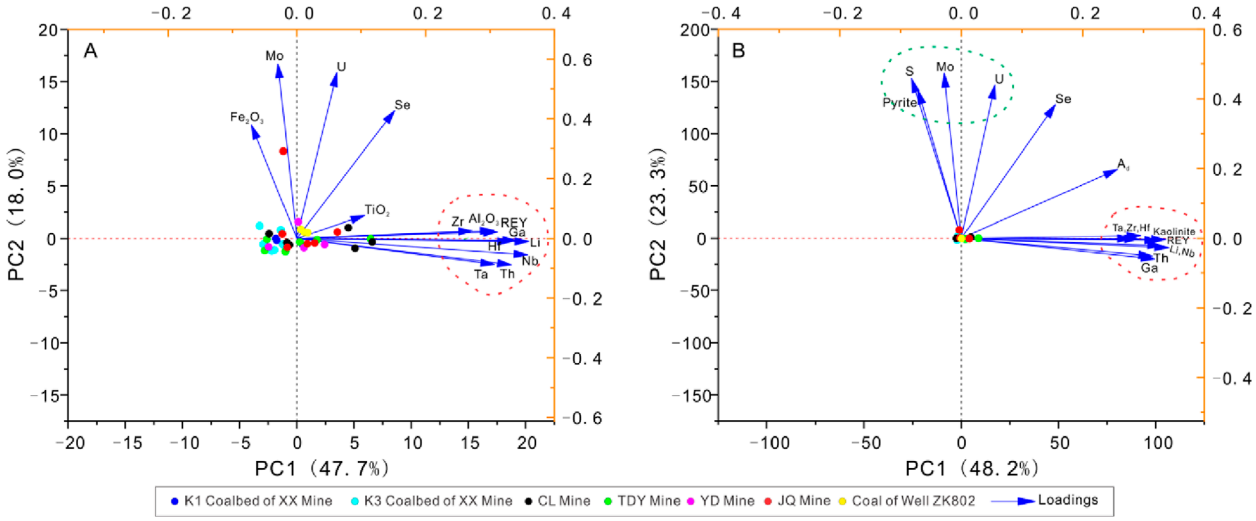

FIGURE 9
Principal component analysis (PCA) of all measured variables in the Late Permian coalfield in northeast Guizhou. Arrows represent variables. **(A)** Comprises major elements and critical elements; **(B)** comprises sulfur content, ash content, mineral composition, and critical elements. Principal component 1 in **(A)** and **(B)** explained 47.7% and 48.2% of the total variances, respectively.

discrimination diagrams are used in this study as these elements appear immobile in our study (Liu et al., 2020).

The coal samples and clay rocks from the Well ZK802, as well as tonstein samples from the K1 Coalbed of XX Mine, all exhibit low Al_2O_3/TiO_2 ratio (3–8) (Figure 10A). In Figure 10B, the data points corresponding to these samples fall within the range of alkaline basalt and are close to Emeishan basalt. In Figure 10C, data points fall within the range of intraplate volcanic rocks, while in Figure 10D, they are close to the low titanium basalt of the Kangdian Upland, suggesting that the inorganic components in this sample come from the low titanium basalt of the Kangdian Upland. These samples have the characteristics of low Ti/Y (427–452) and low Nb/La (0.75–0.82), similar to the low titanium basalt of the Kangdian Upland (Ti/Y<500, and Nb/La ranging between 0.6 and 1.4). It is suggested that the inorganic components in coal samples and overlying clay rocks come from low titanium basalts in the

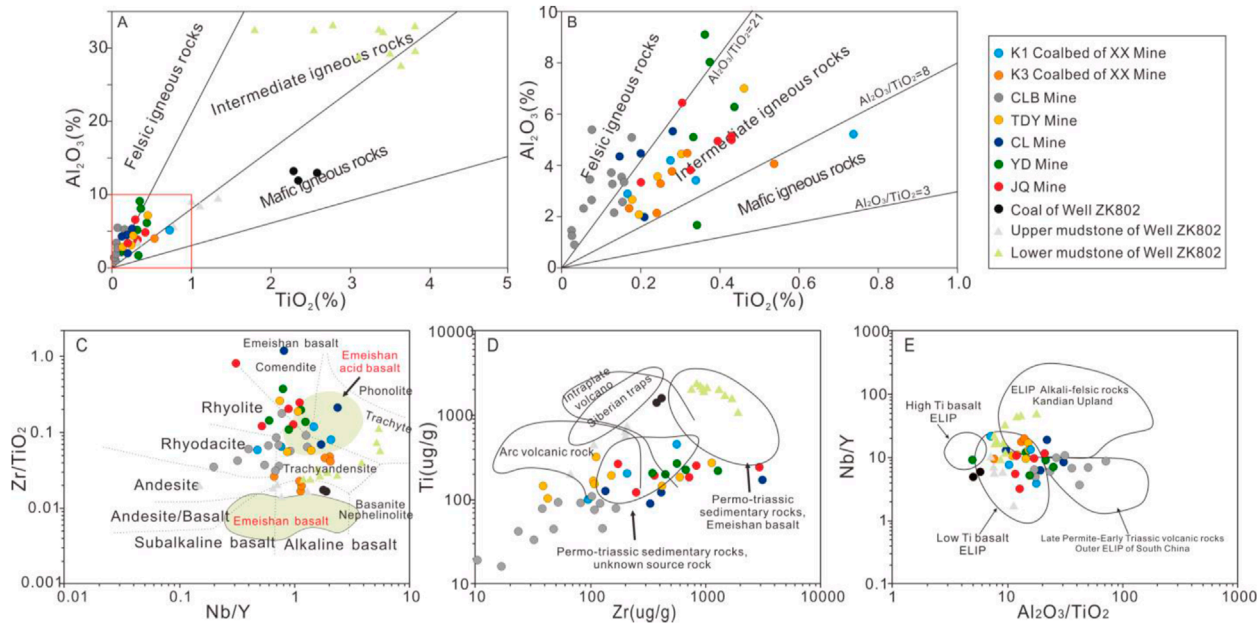

FIGURE 10
Relationship between Al_2O_3 versus TiO_2 **(A, B)**, Zr/TiO_2 versus Nb/Y **(C)**, Ti versus Zr **(D)**. And Nb/Y versus Al_2O_3/TiO_2 **(E)** in the Late Permian coalfield in northeast Guizhou.

Kangdian Upland. In study area, only coal samples from Well ZK802 showed varying degrees of enrichment in Sc, V, Cr, Co., Ni, Cu, Zn, and Se. This enrichment feature was discovered in coal samples from the Late Permian period, which were sourced from Kangdian Upland basalt (Xiao et al., 2004), indirectly confirming the view that the inorganic components in the Well ZK802 samples come from Kangdian Upland basalt.

5.1.3 The input of acidic volcanic ash during the late permian

Except for coal samples and clay rocks from CLB Mine and Well ZK802, almost all data points of other coal samples fall within the range of neutral rocks, indicating that the provenance belongs to neutral rocks (Figures 10A, B). Most studies propose that the characteristics of acidic rocks and intermediate acidic volcanic ash in the Upper Permian strata in Southwest China and the weathering debris input of acidic rocks at the top of the Emeishan basalt are related (Li et al., 2020; Zhao et al., 2019; Liu et al., 2020). Figure 9C shows that most of the coal samples and tonstein samples from TDY, CL, YD, and JQ Mines fell into the rough rock and alkali flow rock areas, and overlapped with the Emeishan acidic volcanic rock area, indicating that the main source of inorganic components in these coal mines is the input of intermediate acidic volcanic ash. In addition, the data points of these samples are concentrated within the range of Permian-Triassic sedimentary rocks with unknown volcanic rock provenance (Figure 10D). Moreover, in Figure 10E, these data points are concentrated in the alkaline rock range of Emeishan, which also implies the presence of volcanic rock provenance. Comparison of REY distribution patterns shows that these coal samples and tonstein samples differ significantly from ELIP felsic intrusive rocks (such as granite and diorite) (Figure 11), but are more similar to alkaline rhyolite, indicating the input of volcanic ash from eruptions rather than the weathering products of felsic intrusive rocks.

The mineral content and morphological characteristics in coal samples also indicate that the inorganic components come from the input of intermediate acidic volcanic ash. The quartz content is low (Table 2), and it has not even been detected in most samples. Under SEM, quartz occurs as extremely fine particles (Figures 4F, G), belonging to authigenic origin rather than terrestrial detrital origin. It has been reported that the intermediate acidic rocks at the top of the Emeishan basalt have a high quartz content (Shellnutt and Jahn, 2010). Quartz deposition in peat bogs can lead to an increase in quartz content in coal seams and surrounding rocks (Liu et al., 2019). In addition, worm-like kaolinite was observed in coal samples (Figure 4E), which also confirms that the provenance belongs to volcanic rocks (Dai et al., 2017). Vertically, the Al_2O_3/TiO_2 of tonstein is significantly higher than that in coal sample, belonging to the range of felsic provenance. This indicates that the increased input of intermediate acidic volcanic ash led to the termination of peat accumulation and the formation of interbedded tonstein (Figures 12D–G). The variation of Al_2O_3/TiO_2 in coal samples is small. However, Al_2O_3/TiO_2 showed high values (>21) in the samples near the tonstein and at the bottom of the coalbed (Figures 12D–G), reflecting input from intermediate acidic volcanic materials.

5.1.4 Input of weathered debris from acidic rocks at the top of ELIP

Most of the sample data points from XX Mine fall within the range of neutral provenance (Figures 10A, B), while a small number of coal samples and tonstein samples fall within the range

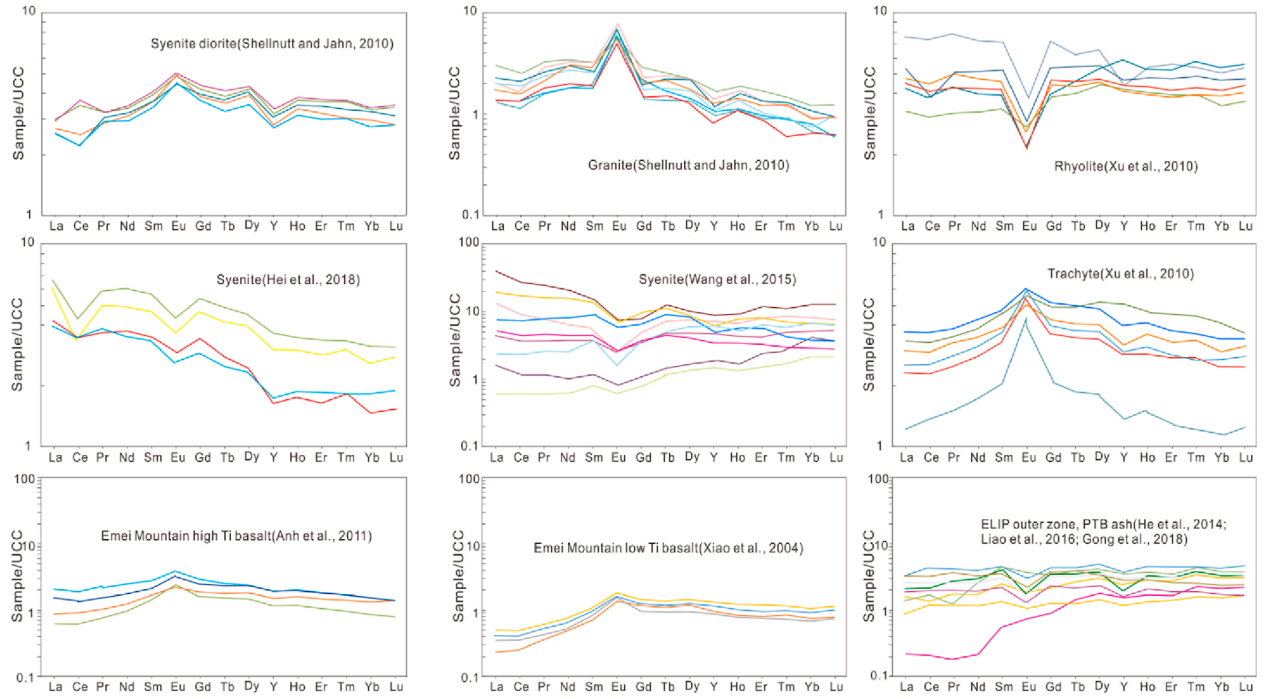

FIGURE 11
ELIP felsic intrusive rocks and volcanic rocks with rare earth element partition model [modified from Li et al. (2020); Shen et al. (2023)].

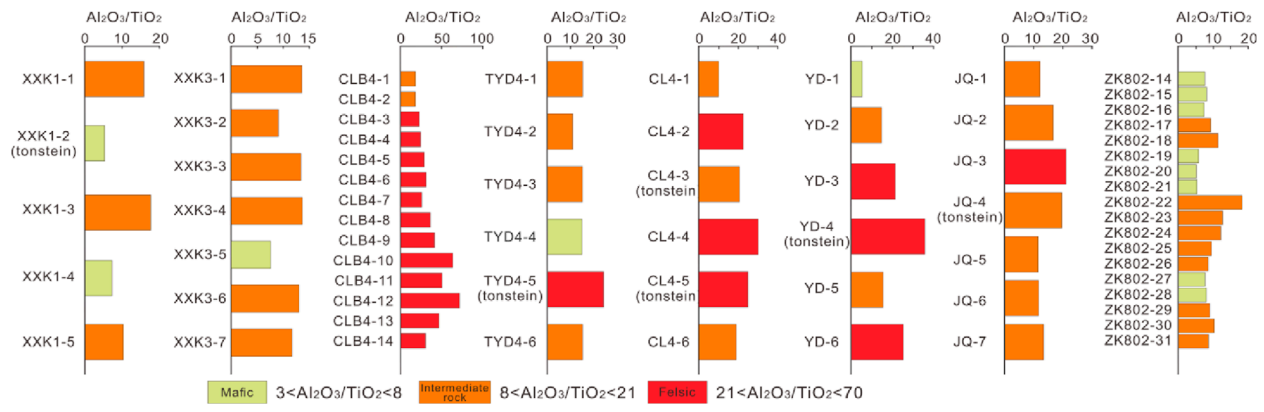

FIGURE 12
Vertical variations of Al_2O_3/TiO_2 of the Late Permian coalfield in northeast Guizhou.

of ferromagnesian provenance. The data points corresponding to the K1 Coalbed are distributed at the common boundary of coarse-grained rock and coarse-grained andesite, as well as at the common boundary of coarse-grained andesite and rhyolite (Figures 10C–E). The tonstein sample is close to the range of Emeishan basalt. The data points corresponding to the K3 Coalbed are distributed within the range of coarse andesite and alkaline basalt. Compared to samples influenced by intermediate acidic volcanic rocks, the samples from XX Mine are closer to the alkaline basalt range. Liu et al. (2019) proposed that the main factor contributing to the enrichment of REY and critical elements in coalfields of western Guizhou Province is the input of alkaline volcanic material from the top of ELIP. It can be inferred that the plagioclase neutral rocks at the top of ELIP are the main provenance of XX Mine (Dai et al., 2016; Xie et al., 2017). Similar to the coal samples from southern Sichuan Province, there is a negative Ce anomaly in the samples from XX Mine, indicating a provenance dominated by felsic or felsic neutral rocks (Dai et al., 2015).

The coal samples from XX Mine have a high quartz content. Quartz particles are large and have a certain degree of roundness, indicating terrestrial debris origin. Meanwhile, some small self-generated quartz particles have also been observed, which are the weathering products of basalt in the Kangdian Upland or siliceous hydrothermal precipitation products (Dai et al., 2012). Vertically,

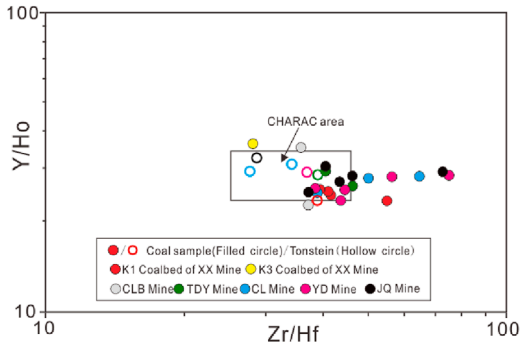

FIGURE 13
Plot of Y/Ho versus Zr/Hf from northeast Guizhou coal field, CHARAC area are modified from Bau M. (1996).

some samples have low Al_2O_3/TiO_2, corresponding data points falling within the range of mafic provenance (Figures 11A, 12B), suggesting terrigenous detrital input from Kangdian Upland basalt.

5.1.5 Volcanic arc or paleozoic orogenic belt

Most of the clay rocks and coal samples from Well ZK802 belong to alkaline basalt (Figure 12E). The low titanium Emeishan basalt exhibits sub-alkaline characteristics, indicating that these samples have other provenance regions. The deposition of alkaline volcanic ash in coal-accumulating environments is an important factor in the enrichment of critical metal elements in Late Permian coal in the study area (Dai et al., 2016; 2017). Some studies have suggested that the felsic inorganic components in coalfields in western Guizhou come from remote volcanic arcs or Paleozoic orogenic belts, rather than ELIP (Liu et al., 2020). The coal samples from CLB Mine have the highest Al_2O_3/TiO_2 content, indicating that the inorganic components come from the input of felsic substances. The Nb/Y-Zr/TiO2 cross-plot indicates the input of alkaline and sub-alkaline intermediate acidic volcanic ash (Figure 10C). The extrusive rocks induced by the Emeishan mantle plume belong to the alkaline - peralkaline category (Hei et al., 2018), providing an alkaline-peralkaline provenance for the study area. The acidic volcanic ash at the Permian-Triassic boundary in southern China provides sub-alkaline volcanic debris (Liao et al., 2016). In Figure 9D, the coal sample from CLB Mine is closer to the arc volcano range, while most of the data points fall within the Late Permian-Early Triassic volcanic rock range (Figure 10E), showing the contribution of more distant volcanic arcs to inorganic components. In the coal samples from CLB Mine, the element enrichment combination is Se-Mo-Ge-Nb-U, which differs significantly from the enrichment combinations of Kangdian Upland basalt, felsic volcanic rocks at the top of basalt, and intermediate acidic volcanic ash, but is similar to two reported coalbeds in western Guizhou Province (Liu et al., 2020). The inorganic components of these two coalbeds are considered to originate from unknown volcanic arcs and/or distal orogenic belts. Vertically, Al_2O_3/TiO_2 shows a decreasing trend, indicating a continuously decreasing input intensity of volcanic arcs and/or distal orogenic belt debris (Figure 12C).

5.2 The influence of hydrothermal fluids

In southwestern China, hydrothermal fluids are an important factor affecting the mineralogy and geochemical anomalies of coal (Dai et al., 2004; 2012). Widespread fluid activity plays an important role in the activation, migration, and enrichment of critical metal elements in coal (Cheng et al., 2015; Li et al., 2017; Yang et al., 2017).

5.2.1 Formation and transformation of minerals

The presence of ammonium illite is direct evidence of high-temperature fluid activity, and it is commonly observed in samples from CLB Mine. Ammonium illite occurs in two ways in coal: 1) illite is formed by alteration through the substitution of NH_4^+ and K^+ (Williams et al., 1992); 2) Kaolinite and nitrogen interact with coalification to form (Dai et al., 2012). Illite was not detected in the CLB Mine samples, therefore the formation of ammonium illite is related to the second way. The nitrogen involved in the formation of ammonium illite may come from bacterial decay and thermal decomposition of organic matter, reacting with H+ to form $NH4^+$. Under reducing and acidic conditions, $NH4^+$ easily enters the pore fluid. Ammonium illite occurs in pores or cell lumen, coexisting with kaolinite, indicating that ammonium illite may originate from the kaolinite precursor produced by the interaction between kaolinite and $NH4^+$ during coalification process (Williams et al., 1989; 1992).

Kaolinite was detected in coal and tonstein samples from TDY, YD, CL, and XX mines, while other types of clay minerals were not detected. However, various types of clay minerals were detected in the samples of CLB, JQ Mine, and Well ZK802. The clay minerals in the coal samples of study area are mainly kaolinite, which is induced by the decomposition of debris in the highly acidic solution of peat swamp, promoting the transformation of other aluminosilicates into kaolinite. In the coal sample from Well ZK802, zeolite is also evidence of low-temperature hydrothermal fluid activity. Letoshite is mainly formed in some low-temperature hydrothermal alteration zones and widely replaces potassium feldspar along this vein, or it may have been formed during low-grade metamorphism (Susilawati and Ward, 2006). Kaolinite, montmorillonite, zeolite, and plagioclase can all form zeolite through weathering. The process of kaolinite deformation into zeolite requires additional material supply, including SiO_2, Na^+, and K^+, and the most likely provider of these substances is hydrothermal fluid (Hower and Gayer, 2002). Due to the fact that the coal sample mainly contains kaolinite and quartz, this indicates that zeolite is mainly formed through low-temperature hydrothermal alteration.

Carbonate minerals and sulfate minerals can also confirm hydrothermal fluid activity. Calcite is widely distributed in various coalbeds in the study area. Except for CL Mine, no carbonate minerals were detected in the tonstein and floor samples of other mines. Calcite mainly appears in the form of fracture cement in coal (Figure 4H). The fractures formed after coalbed rupture provide permeable channels for Ca^{2+} rich hydrothermal fluids to pass through the coalbed (rather than the tonstein). The gypsum content that occurs as fracture cement is low and coexists with pyrite (Figures 4I–K). Iron sulfides near fractures are easily oxidized, and fluids rich in oxygen and calcium may be more likely to promote the production of iron containing sulfate minerals along fractures (Figure 4L) (Dai et al., 2013). In addition, the authigenic small quartz (Figure 4F), fracture-cemented pyrite

TABLE 6 The maximum and minimum values of Nb/Ta and Zr/Hf in coal samples from the Late Permian coalfield in northeast Guizhou.

Mine/Well	XX (K1 coalbed)	XX (K3 coalbed)	CLB	TDY	CL	YD	JQ	ZK802
Nb/Ta	17–22	9–18	27	14–33	12–119	9–33	10–50	18–29
Zr/Hf	39–56	35–46	35–69	35–56	29–66	38–77	29–75	35–47

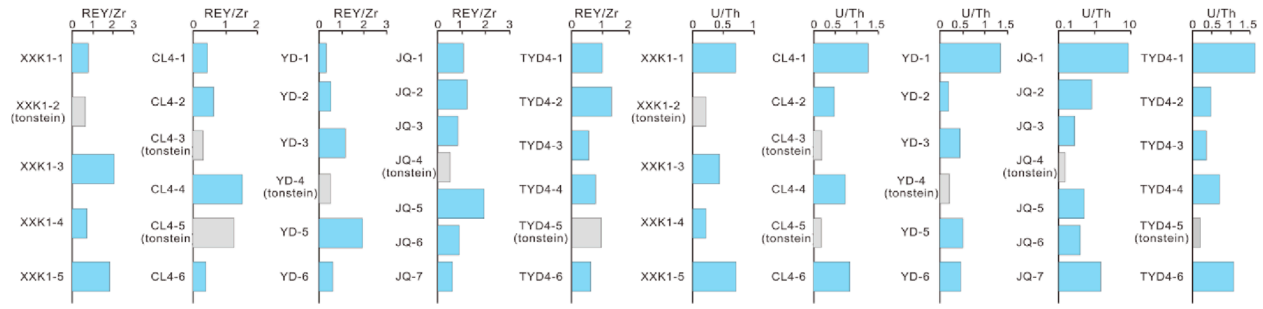

FIGURE 14
Vertical variation of REY/Zr and U/Th in coal samples from the Late Permian coalfield in northeast Guizhou.

(Figure 4L), and authigenic siderite (Figure 4J) all suggest the input of hydrothermal fluids.

5.2.2 Activation and migration of enriched elements

As a high field strength element, Nb-Ta-Zr-Hf-REY is believed to not migrate under low-temperature hydrothermal conditions (Arbuzov et al., 2019), migration occurs only under the action of strong acidic hydrothermal solution (Spears and Arbuzov, 2019). In Figure 13, all data points of the tonstein samples fall within the CHARAC range. Some data points of coal samples fall outside the CHARAC range, indicating that the fluid has fractionated Zr-Hf and Y-Ho (Bau M.,1996). For samples from different coal mines, Nb/Ta and Zr/Hf vary greatly, especially in CL, YD, and JQ coal mines (Table 6). Under the action of acidic fluid, the two elements with strong migration ability, Nb and Zr, undergo migration, resulting in fractionation of the combination of Nb-Ta and Zr-Hf elements. The Nb/Ta and Zr/Hf ratios in the coal samples are higher than those in the tonstein sample, indicating that Nb and Zr are relatively more actively leached from the tonstein and then deposited in the underlying organic matter. The re-deposition of elements is the reason for the enrichment of Nb and Zr in multiple coalfields in southwestern China (Dai et al., 2013). Meanwhile, few samples in the present study are characterized by Gd-maximum as well as MREY enrichment (Figures 8A, B), which is indicative of acid solutions (e.g., high P_{CO2}-waters) (Shand et al., 2005).

Compared to Nb, Ta, Zr, and Hf, REY has a higher mobility in aqueous solutions (Liu et al., 2019). Therefore, the vertical variation of REY content is inconsistent with Nb, Ta, Zr, and Hf. In XX, CL, YD, and JQ coal mines, the REY/Zr ratio of the interbedded tonstein is lower than that of the underlying coalbed (Figure 14), indicating that some REY leaches out of the interbedded tonstein and subsequently re-enriches in the underlying coalbed. Meanwhile, in the tonstein of TDY and CL coal mines, the REY/Zr ratio is higher than that of the underlying coalbed (Figures 14B, E), indicating that the overlying coalbed provides a source of REY. Under the action of gravity, fluids rich in REY enter the underlying tonstein. However, due to the barrier effect or changes in acidity or alkalinity, REY precipitates in the tonstein and no longer penetrates downwards. Acidic water can cause leaching and migration of REY, while alkaline water can cause re-precipitation of REY. The variation of U/Th can be used to reflect the migration and re deposition of acidic aqueous solutions between coalbeds and tonstein. In all coalbeds, the U/Th of the interbedded tonstein is lower than that of the underlying coal sample, indicating that U leaches out of the interbedded tonstein and then re precipitates in the underlying coalbed. It is worth noting that in the samples from the top of the coalbed, U/Th is higher than in other positions. This reflects the leaching of U elements from the overlying roof, which entered the top coalbed and led to an increase in U/Th. In addition, the roof composed of carbonate rock is easily influenced by seawater and may contain a high content of U, which may also lead to a high U content in the coalbed.

5.3 The influence of seawater

Wang et al. (2008) proposed that the variations in REY content in coal are due to the mixing of weathering products of Emeishan basalt under the influence of regression and transgression. Coalbeds formed in environments less affected by seawater have relatively high levels of REY. Previous studies have shown that coal affected by the ocean has a higher sulfur content than coal formed in freshwater environments (Chou, 2012). In this study, the total sulfur content of coal samples is between 1.1% and 24%, belonging to medium-high sulfur coal. Sulfur mainly occurs as pyrite (Figure 9B), with a small amount occurring as organic matter and sulfate. The occurrence form of pyrite implies the influence of seawater. The Sr/Ba value has been successfully used as a marine-influence indicator for

peat depositional environments, with Sr/Ba>1 indicating a marine influence for coal samples (Spiro et al., 2019). In this study, the Sr/Ba ratio of most coal samples was higher than 1, indicating that the coalbed was affected by seawater. The diffusion of varying degrees of seawater into peat bogs may lead to changes in the mineralogical and geochemical patterns of coal, as well as the enrichment of marine derived elements. In this study, the correlation between Se, U, and Mo with Nb, Ta, Zr, Hf, and REY was weak, but the correlation between Se and U, S was good (Figure 9B), indicating that Se may be related to sulfides represented by pyrite. The formation of pyrite is influenced by seawater, therefore the enrichment of Se and U in coal is also related to the influence of seawater.

6 Conclusion

(1) The chemical composition of coal from the Late Permian Wujiaping Formation in northeastern Guizhou is characterized by ultra-low moisture content, moderate ash content, moderate volatile matter yield, and medium high sulfur content. These coal samples are composed of clay minerals (including kaolinite, illite, ammonium illite, etc.), quartz, rutile, pyrite, calcite, gypsum and other minerals. There are certain differences in mineral composition among coal samples from different coal mines. The content of critical metal elements in coal is high, and the elemental composition of different minerals varies greatly. Vertically, critical metal elements are enriched in the tonstein and nearby coalbeds.

(2) The input of terrestrial debris is the main factor affecting the abundance of critical metal elements in coal, and the weathering products of acidic volcanic ash, basalt, and intermediate acidic rocks in the Kangdian Upland provide the material sources of critical metal elements. The input of intermediate acidic volcanic ash is the main factor for the enrichment of Nb-Ta-Zr-Hf-REY in most coal mines. The coastal swamp environment of the transitional facies, seawater infiltration, and hydrothermal fluids control the alteration and transformation of detrital minerals and the precipitation of authigenic minerals. The activation and migration of some critical metal elements are also controlled by these factors.

Data availability statement

The raw data supporting the conclusions of this article will be made available by the authors, without undue reservation.

Author contributions

ZY: Conceptualization, Investigation, Visualization, Writing–original draft. BL: Investigation, Methodology, Supervision, Writing–original draft. JC: Methodology, Resources, Supervision, Visualization, Writing–review and editing.

Funding

The author(s) declare that financial support was received for the research, authorship, and/or publication of this article. This study was funded by the National Natural Science Foundation of China (No. 41972182).

Conflict of interest

The authors declare that the research was conducted in the absence of any commercial or financial relationships that could be construed as a potential conflict of interest.

Generative AI statement

The author(s) declare that no Generative AI was used in the creation of this manuscript.

Publisher's note

All claims expressed in this article are solely those of the authors and do not necessarily represent those of their affiliated organizations, or those of the publisher, the editors and the reviewers. Any product that may be evaluated in this article, or claim that may be made by its manufacturer, is not guaranteed or endorsed by the publisher.

References

Arbuzov, S. I., Spears, D. A., Vergunov, A. V., Ilenok, S. S., Mezhibor, A. M., Ivanov, V. P., et al. (2019). Geochemistry, mineralogy and genesis of rare metal (Nb-Ta-Zr-Hf-Y-REE-Ga) coals of the seam XI in the south of kuznetsk basin, Russia. *Ore Geol. Rev.* 113, 103073. doi:10.1016/j.oregeorev.2019.103073

ASTM Standard D3173/D3173M – 17a (2017). *Standard test method for moisture in the analysis sample of coal and coke*. West Conshohocken, PA: ASTM International.

ASTM Standard D3174-12 (Reapproved 2018) (2018). *Ash in the analysis sample of coal and coke from coal*. West Conshohocken, PA: ASTM International.

ASTM Standard D3175-17 (2011). *Standard test method for volatile matter in the analysis sample of coal and coke*. West Conshohocken, PA: ASTM International.

Bau, M. (1996). Controls on the fractionation of isovalent trace elements in magmatic and aqueous systems: evidence from Y/Ho, Zr/Hf, and lanthanide tetrad effect. *Contributions Mineralogy and Petrology* 123, 323–333. doi:10.1007/s004100050159

Boehme, J., Coble, P., Conmy, R., and Stovall-Leonard, A. (2004). Examining CDOM fluorescence variability using principal component analysis: seasonal and regional modeling of three-dimensional fluorescence in the Gulf of Mexico. *Mar. Chem.* 89, 3–14. doi:10.1016/j.marchem.2004.03.019

China Coal Geology Bureau (1996). "Sedimentary environments and coal accumulation of late permian coal Formation in western Guizhou," in *Southern sichuan and eastern yunnan*. China: Chongqing University Press. Ch.

Chou, C. L. (2012). Sulfur in coals: a review of geochemistry and origins. *Int. J. Coal Geol.* 100, 1–13. doi:10.1016/j.coal.2012.05.009

Chung, F. K. (1974). Quantitative interpretation of X-ray diffraction patterns of mixtures. II. Adiabatic principle of X-ray diffraction analysis of mixtures. *J. Appl. Crystallogr.* 7, 526–531. doi:10.1107/S0021889874010387

Crowley, S. S., Ruppert, L. F., Belkin, H. E., Stanton, R. W., and Moore, T. A. (1993). Factors affecting the geochemistry of a thick, subbituminous coal bed in the Powder

River Basin: volcanic, detrital, and peat-forming processes. *Org. Geochem.* 20 (6), 843–853. doi:10.1016/0146-6380(93)90067-L

Dai, S., Li, D., Ren, D., Tang, Y., Shao, L., and Song, H. (2004). Geochemistry of the late Permian No. 30 coal seam, Zhijin Coalfield of Southwest China: influence of a siliceous low-temperature hydrothermal fluid. *Appl. Geochem.* 19 (2004), 1315–1330. doi:10.1016/j.apgeochem.2003.12.008

Dai, S., Liu, C., Zhao, L., Liu, J., Wang, C., and Ren, D. (2022). Strategic metal mineral resources in coal measures: significance and challenges. *J. China Coal Sci.* 47 (5), 1743–1749. doi:10.13225/j.cnki.jccs.MJ22.0011

Dai, S., Liu, J., Ward, C. R., Hower, J. C., French, D., Jia, S., et al. (2015). Mineralogical and geochemical compositions of Late Permian coals and host rocks from the Guxu Coalfield, Sichuan Province, China, with emphasis on enrichment of rare metals. *Int. J. Coal Geol.* 166, 71–95. doi:10.1016/j.coal.2015.12.004

Dai, S., Ren, D., Chou, C., Finkelman, R., Seredin, V., and Zhou, Y. (2012). Geochemistry of trace elements in Chinese coals: a review of abundances, genetic types, impacts on human health, and industrial utilization. *Int. J. Coal Geol.* 94, 3–21. doi:10.1016/j.coal.2011.02.003

Dai, S., Ren, D., Tang, Y., Yue, M., and Hao, L. (2005). Concentration and distribution of elements in late permian coals from western Guizhou province, China. *Int. J. Coal Geol.* 61, 119–137. doi:10.1016/j.coal.2004.07.003

Dai, S., Shen, M., Liu, G., and Zhao, L. (2024). Enrichment mechanism of rare earth elements in Late Permian coal measure basement tuff in western Guizhou. *Acta Geol. Sin.* 98 (8), 2316–2335. doi:10.19762/j.cnki.dizhixuebao.2024188

Dai, S., Ward, C. R., Graham, I. T., French, D., Hower, J. C., Zhao, L., et al. (2017). Altered volcanic ashes in coal and coal-bearing sequences: a review of their nature and significance. *Earth-Science Rev.* 175, 44–74. doi:10.1016/j.earscirev.2017.10.005

Dai, S., Xie, P., Jia, S., Ward, C. R., Hower, J. C., Yan, X., et al. (2016). Enrichment of U-Re-V-Cr-Se and rare earth elements in the Late Permian coals of the Moxinpo Coalfield, Chongqing, China: genetic implications from geochemical and mineralogical data. *Ore Geol. Rev.* 80, 1–17. doi:10.1016/j.oregeorev.2016.06.015

Dai, S., Zhang, W., Ward, C. R., Seredin, V. V., Hower, J. C., Li, X., et al. (2013). Mineralogical and geochemical anomalies of late Permian coals from the Fusui Coalfield, Guangxi Province, southern China: influences of terrigenous materials and hydrothermal fluids. *Int. J. Coal Geol.* 105, 60–84. doi:10.1016/j.coal.2012.12.003

Dai, S., Zhao, L., Wei, Q., Song, X., Wang, W., Liu, J., et al. (2020). Resources of critical metals in coal-bearing sequences in China: enrichment types and distribution. *Sci. China Press* 65 (33), 3715–3729. doi:10.1360/TB-2020-0112

Finkelman, R. B., Dai, S., and French, D. (2019). The importance of minerals in coal as the hosts of chemical elements: a review. *Int. J. Coal Geol.* 212, 103251. doi:10.1016/j.coal.2019.103251

Finkelman, R. B., Palmer, C. A., and Wang, P. P. (2018). Quantification of the modes of occurrence of 42 elements in coal. *Int. J. Coal Geol.* 185, 138–160. doi:10.1016/j.coal.2017.09.005

GBT 15224.1-2018 (2018). "Classification for quality of coal in P.R. China," in *Part 1 ash*.

Gotelli, N. J., and Ellison, A. M. (2004). *A primer of ecological statistics*. Sunderland, MA: Sinauer Associates.

Hayashi, K., Fujisawa, H., Holland, H. D., and Ohmoto, H. (1997). Geochemistry of ~1.9 Ga sedimentary rocks from northeastern Labrador, Canada. *Geochimica Cosmochimica Acta* 61 (19), 4115–4137. doi:10.1016/S0016-7037(97)00214-7

He, B., Xu, Y. G., Chung, S. L., Xiao, L., and Wang, Y. M. (2003). Sedimentary evidence for a rapid, kilometer-scale crustal doming prior to the eruption of the Emeishan flood basalts. *Earth Planet. Sci. Lett.* 213, 391–405. doi:10.1016/S0012-821X(03)00323-6

Hei, H., Su, G., Wang, Y., Mo, X., Luo, Z., and Liu, W. (2018). Rhyolites in the emeishan large igneous province (SW China) with implications for plume-related felsic magmatism. *J. Asian Earth Sci.* 164, 344–365. doi:10.1016/j.jseaes.2018.05.032

Hower, J., Eble, C., O'Keefe, J., Dai, S., Wang, P., Xie, P., et al. (2015). Petrology, palynology, and geochemistry of gray hawk coal (early pennsylvanian, langsettian) in eastern Kentucky, USA. *Minerals* 5 (3), 592–622. doi:10.3390/min5030511

Hower, J. C., Cantando, E., Eble, C. F., and Copley, G. C. (2019). Characterization of stoker ash from the combustion of high-lanthanide coal at a Kentucky bourbon distillery. *Int. J. Coal Geol.* 213, 103260. doi:10.1016/j.coal.2019.103260

Hower, J. C., and Gayer, R. A. (2002). Mechanisms of coal metamorphism: case studies from Paleozoic coalfields. *Int. J. Coal Geol.* 50, 215–245. doi:10.1016/S0166-5162(02)00119-2

Iwamori, H., Yoshida, K., Nakamura, H., Kuwatani, T., Hamada, M., Haraguchi, S., et al. (2017). Classification of geochemical data based on multivariate statistical analyses: complementary roles of cluster, principal component, and independent component analyses. *Geochem. Geophys. Geosystems* 18 (3), 994–1012. doi:10.1002/2016GC006663

Jin, C., Liu, L., Zhang, X., Gao, S., Cheng, Z., Li, B., et al. (2024). Characteristics and genetic mechanism of Li- Nb- Ta enrichment in Late Permian coal in the coalfield of northwestern Guizhou, Southwest China. *Acta Geol. Sin.* 98 (8), 2316–2335. doi:10.19762/j.cnki.dizhixuebao.2024188

Ketris, M. P., and Yudovich, Y. (2009). Estimations of Clarkes for Carbonaceous biolithes: world averages for trace element contents in black shales and coals. *Int. J. Coal Geol.* 78, 135–148. doi:10.1016/j.coal.2009.01.002

Lattin, J. M., Carroll, J. D., Green, P. E., and Green, P. E. (2003). *Analyzing multivariate data*. Pacific Grove, CA: Thomson Brooks/Cole.

Li, B., Zhaung, X., Querol, X., Li, J., Moreno, N., Córdoba, P., et al. (2019). Geological controls on enrichment of Mn, Nb (Ta), Zr (Hf), and REY within the early permian coals of the jimunai depression, xinjiang province, NW China. *Int. J. Coal Geol.* 215, 103298. doi:10.1016/j.coal.2019.103298

Li, B., Zhuang, X., Li, J., Querol, X., Font, O., and Moreno, N. (2017). Enrichment and distribution of elements in the late permian coals from the zhina coalfield, Guizhou province, southwest China. *Int. J. Coal Geol.* 171, 111–129. doi:10.1016/j.coal.2017.01.003

Li, B., Zhuang, X., Ning, S., Li, J., Wang, X., Huang, S., et al. (2022). Mobilization, migration and enrichment mechanism of zr (Hf)-Nb(Ta)-Ga rare earth elements: a case study of the coal bearing strata of the Upper Permian Wujiaping Formation in Wuzhengdao Area. *J. China Coal Soc.* 47 (5), 1822–1839. doi:10.13225/j.cnki.jccs.MJ22.0136

Li, B., Zhuang, X., Querol, X., Moreno, N., Córdoba, P., Shangguan, Y., et al. (2020). Geological controls on the distribution of REY-Zr (Hf)-Nb (Ta) enrichment horizons in late Permian coals from the Qiandongbei Coalfield, Guizhou Province, SW China. *Int. J. Coal Geol.* 231, 103604. doi:10.1016/j.coal.2020.103604

Liu, J., Song, H., Dai, S., Nechaev, V. P., Graham, I. T., French, D., et al. (2019). Mineralization of REE-Y-Nb-Ta-Zr-Hf in wuchiapingian coals from the liupanshui coalfield, Guizhou, southwestern China: geochemical evidence for terrigenous input. *Ore Geol. Rev.* 115, 103190. doi:10.1016/j.oregeorev.2019.103190

Liu, J. J., Nechaev, V. P., Dai, S., Song, H., Nechaeva, E. V., Jiang, Y., et al. (2020). Evidence for multiple sources for inorganic components in the Tucheng coal deposit, western Guizhou, China and the lack of critical-elements. *Int. J. Coal Geol.* 223, 103468. doi:10.1016/j.coal.2020.103468

Martin, G., Rentsch, L., H¨ock, M., and Bertau, M. (2017). Lithium market research – global supply, future demand and price development. *Energy Storage Mater.* 6, 171–179. doi:10.1016/j.ensm.2016.11.004

Meglen, R. R. (1992). Examining large databases: a chemometric approach using principal component analysis. *Mar. Chem.* 39, 217–237. doi:10.1016/0304-4203(92)90103-H

MT/T 849–2000 (National Standard of P.R. China), 2000. Classification for volatile matter of coal.

MT/T 850–2000 (National Standard of P.R. China), 2000. Classification for moisture of coal.

Per, K., and Erika, M. (2018). Examining the rare-earth elements (REE) supply–demand balance for future global wind power scenarios. *Geol. Surv. Den. Greenl. Bull.* 41, 87–90. doi:10.34194/geusb.v41.4350

Querol, X., Whateley, M. K. G., Fernfindez-Turiel, J. L., and Tuncali, E. (1997). Geological controls on the mineralogy and geochemistry of the Beypazari lignite, central Anatolia, Turkey. *Int. J. Coal Geol.* 33, 255–271. doi:10.1016/S0166-5162(96)00044-4

Ren, D. Y. (2006). *Geochemistry of trace elements in coal*. Beijing, China: Science Press.

Seredin, V. V., and Dai, S. (2012). Coal deposits as potential alternative sources for lanthanides and yttrium. *Int. J. Coal Geol.* 94, 67–93. doi:10.1016/j.coal.2011.11.001

Seredin, V. V., and Finkelman, R. B. (2008). Metalliferous coals: a review of the main genetic and geochemical types. *Int. J. Coal Geol.* 76, 253–289. doi:10.1016/j.coal.2008.07.016

Shand, P., Johannesson, K. H., Chudaev, O., Chudaeva, V., and Edmunds, W. M. (2005). "Rare earth element contents of high pCO2 groundwaters of Primorye, Russia: mineral stability and complexation controls," in *Rare earth elements in groundwater flo* (Netherlands: Springer).

Shellnutt, J. G., and Jahn, B. M. (2010). Formation of the Late Permian Panzhihua plutonic-hypabyssal-volcanic igneous complex: implications for the genesis of Fe–Ti oxide deposits and A-type granites of SW China. *Earth Planet. Sci. Lett.* 289, 509–519. doi:10.1016/j.epsl.2009.11.044

Shen, M., Dai, S., Graham, I. T., Nechaev, V. P., French, D., Zhao, F., et al. (2021). Mineralogical and geochemical characteristics of altered volcanic ashes (tonsteins and K-bentonites) from the latest Permian coal-bearing strata of western Guizhou Province, southwestern China. *Int. J. Coal Geol.* 237, 103707. doi:10.1016/j.coal.2021.103707

Shen, M. L., Dai, S. F., Nechaev, V. P., French, D., Graham, I. T., Liu, S. D., et al. (2023). Provenance changes for mineral matter in the latest Permian coals from western Guizhou, southwestern China, relative to tectonic and volcanic activity in the Emeishan Large Igneous Province and Paleo-Tethys region. *Gondwana Res.* 113, 71–88. doi:10.1016/j.gr.2022.10.011

Spears, D. A., and Arbuzov, S. I. (2019). A geochemical and mineralogical update on two major tonsteins in the UK Carboniferous Coal Measures. *Int. J. Coal Geol.* 210, 103199. doi:10.1016/j.coal.2019.05.006

Spiro, B. F., Liu, J., Dai, S., Zeng, R., Large, D., and French, D. (2019). Marine derived $^{87}Sr/^{86}Sr$ in coal, a new key to geochronology and palaeoenvironment: elucidation of

the India-Eurasia and China-Indochina collisions in Yunnan, China. *Int. J. Coal Geol.* 215, 103304. doi:10.1016/j.coal.2019.103304

Susilawati, R., and Ward, C. R. (2006). Metamorphism of mineral matter in coal from the Bukit Asam deposit, south Sumatra, Indonesia. *Int. J. Coal Geol.* 68, 171–195. doi:10.1016/j.coal.2006.02.003

Taylor, S. R., and Mclennan, S. H. (1985). *The continental Crust: its composition and evolution*. Oxford: Blackwell.

Wang, Q., Yang, R., and Miao, B. (2008). Rare earth elements stratigraphic significance in late Permian coal measure from Bijie City, Guizhou Province, China. *J. rare earths* 26 (5), 760–764. doi:10.1016/S1002-0721(08)60178-7

Wang, X., Dai, S., Chou, C., Zhang, M., Wang, J., Song, X., et al. (2012). Mineralogy and geochemistry of late permian coals from the taoshuping mine, yunnan province, China: evidences for the sources of minerals. *Int. J. Coal Geol.* 96-97, 49–59. doi:10.1016/j.coal.2012.03.004

Ward, C. R. (2016). Analysis, origin and significance of mineral matter in coal: an updated review. *Int. J. Coal Geol.* 165, 1–27. doi:10.1016/j.coal.2016.07.014

Williams, L. B., Ferrell, R. E., Chinn, E. W., and Sassen, R. (1989). Fixed-ammonium in clays associated with crude oils. *Appl. Geochem.* 4 (6), 605–616. doi:10.1016/0883-2927(89)90070-X

Williams, L. B., Wilcoxon, B. R., Ferrell, R. E., and Sassen, R. (1992). Diagenesis of ammonium during hydrocarbon maturation and migration, Wilcox Group, Louisiana, U.S.A. *Appl. Geochem.* 7 (2), 123–134. doi:10.1016/0883-2927(92)90031-W

Winchester, J. A., and Floyd, P. A. (1977). Geochemical discrimination of different magma series and their differentiation products using immobile elements. *Chem. Geol.* 20, 325–343. doi:10.1016/0009-2541(77)90057-2

Xiao, L., Xu, Y., Mei, H., Zheng, Y., He, B., and Pirajno, F. (2004). Distinct mantle sources of low-Ti and high-Ti basalts from the western Emeishan large igneous province, SW China: implications for plume–lithosphere interaction. *Earth Planet. Sci. Lett.* 228, 525–546. doi:10.1016/j.epsl.2004.10.002

Xie, P., Zhang, S., Wang, Z., Wang, L., and Xu, Y. (2017). Geochemical characteristics of the Late Permian coals from the Yueliangtian Coalfield, western Guizhou, southwestern China. *Arabian J. Geosciences* 10 (5), 98. doi:10.1007/s12517-017-2916-1

Xue, J., Lee, C., Wakeham, S. G., and Armstrong, R. A. (2011). Using principal components analysis (PCA) with cluster analysis to study the organic geochemistry of sinking particles in the ocean. *Org. Geochem.* 42, 356–367. doi:10.1016/j.orggeochem.2011.01.012

Yamashita, Y., and Tanoue, E. (2003). Distribution and alteration of amino acids in bulk DOM along a transect from bay to oceanic waters. *Mar. Chem.* 82, 145–160. doi:10.1016/S0304-4203(03)00049-5

Yang, R., Cheng, W., Gao, J., Chen, J., Wei, H., Shen, M., et al. (2017). U, Li, Nb and V Element Enrichment of Coal Seams and Potential Resource Evaluation in Southwest Guizhou. *Guizhou Geol.* 34 (2), 77–81. doi:10.3969/j.issn.1000-5943.2017.02.003

Yang, R. D., Liu, L., Wei, H. R., Cui, Y. C., and Cheng, W. (2011). Geochemical characteristics of Guizhou Permian coal measure strata and analysis of the control factors. *J. Coal Sci. and Eng.* 17 (1), 55–68. doi:10.1007/s12404-011-0112-6

Zhai, M., Wu, F., Hu, R., Jiang, S., Li, W., Wang, R., et al. (2019). Critical metal mineral resources: current research status and scientific issue. *Sci. Found. China* 33 (2), 116–111. CNKI:SUN:ZKJJ.0.2019-02-002.

Zhang, Y., Cheng, W., Yang, R., Yang, B., Lv, F., Luo, C., et al. (2023). A review on the abnormal enrichment of some metals in coals from Guizhou. *Geol. Rev.* 69 (1), 247–265. doi:10.16509/j.georeview.2022.10.045

Zhao, L., Dai, S., Nechaev, V. P., Nechaeva, E. V., Graham, I. T., French, D., et al. (2019). Enrichment of critical elements (Nb-Ta-Zr-Hf-REE) within coal and host rocks from the Datanhao mine, Daqingshan Coalfield, northern China. *Ore Geol. Rev.* 111, 102951. doi:10.1016/j.oregeorev.2019.102951

Zhou, J. H., Chen, H. Y., Zhao, L., Wang, X. H., Li, H., Li, T., et al. (2023). Enrichment of critical elements (Li-Ga-Nb-Ta-REE-Y) in the coals and host rocks from the Daping Mine, Yudongnan Coalfield, SW China. *Ore Geol. Rev.* 152, 105245. doi:10.1016/j.oregeorev.2022.105245

Zhuang, X. G., Querol, X., Zeng, R. S., Xu, W. D., Alastuey, A., Lopez-Soler, A., et al. (2000). Mineralogy and geochemistry of coal from the Liupanshui mining district, Guizhou, south China. *Int. J. Coal Geol.* 45, 21–37. doi:10.1016/S0166-5162(00)00019-7